Model Proton-Coupled Electron Transfer Reactions in Solution: Predictions of Rates, Mechanisms, and Kinetic Isotope Effects

Hélène Decornez and Sharon Hammes-Schiffer*

Department of Chemistry, 152 Davey Laboratory, The Pennsylvania State University, University Park, Pennsylvania 16802

Received: May 31, 2000; In Final Form: August 1, 2000

This paper presents a comprehensive theoretical study of model systems directed at predicting the effects of solute and solvent properties on the rates, mechanisms, and kinetic isotope effects for proton-coupled electron transfer (PCET) reactions. These studies are based on a multistate continuum theory in which the solute is described with a multistate valence bond model, the solvent is represented as a dielectric continuum, and the active electrons and transferring protons are treated quantum mechanically. This theoretical formulation is capable of describing a range of mechanisms, including single electron transfer and sequential or concerted EPT mechanisms in which both an electron and a proton are transferred. The probability of the EPT mechanism is predicted to increase as (1) the electron donor−acceptor distance is decreased, (2) the proton donor−acceptor distance is decreased, (3) the proton transfer reaction becomes more exothermic, (4) the electron transfer reaction becomes more endothermic (in the normal Marcus region), (5) the temperature decreases, (6) the solvent polarity decreases, and (7) the size of the electron donor and acceptor increases. The rates are predicted to increase with respect to these properties in a similar manner, with the exception that the rates will increase as the temperature increases and as the electron transfer reaction becomes more exothermic in the normal Marcus region. The kinetic isotope effects are predicted to increase as the probability of the EPT mechanism increases and as the localization and the distance between the reactant and product proton vibrational wave functions increase. Unusually strong kinetic isotope effects may be observed due to strong coupling between the transferring electron and proton. These theoretical studies elucidate the fundamental principles of PCET reactions and provide predictions that can be tested experimentally.

I. Introduction

Proton-coupled electron transfer (PCET) reactions play a critical role in a variety of biological and chemical processes. The conversion of energy during photosynthesis[1] and respiration[2] relies on PCET. In particular, the coupling between the proton motion and electron transfer plays a key role in the proton pumping mechanism of photosynthetic reaction centers,[1] as well as in the conduction of electrons in cytochrome *c*.[3] PCET is also important in numerous reactions in proteins such as ribonucleotide reductase enzyme[4] and iron sulfur proteins.[5] Furthermore, PCET reactions occur in electrochemical processes[6,7] and in solid state materials.[8] Thus, PCET reactions are prevalent in a wide range of systems.

A number of model compounds have been investigated experimentally to elucidate the fundamental principles of PCET reactions. Nocera and co-workers have performed experiments in which they photoinduce electron transfer within an electron donor−acceptor pair connected by a proton transfer interface.[9−11] They have studied a variety of complexes, including a system in which an electron transfers from a Ru(II) polypyridine to a dinitrobenzene through an amidinium−carboxylate proton transfer interface. For this system, they found that the rate of electron transfer changed by nearly 2 orders of magnitude when the proton transfer interface was switched (i.e., carboxylate−amidinium instead of amidinium−carboxylate).[11] In addition to these studies of photoinduced PCET, Meyer and co-workers have performed detailed kinetics studies of ground state PCET reactions in oxoruthenium polypyridyl complexes.[12] In some cases, they measured large kinetic isotope effects (i.e., the ratio of the rate for hydrogen to the rate for deuterium) of ∼30. Thorp and co-workers have studied the effects of substitutions for reactions involving oxoruthenium and also measured large kinetic isotope effects of ∼12.[13] Mayer and co-workers have studied PCET in self-exchange reactions between bi-imidazoline iron complexes.[14] They obtained mechanistic evidence for concerted PCET and measured a kinetic isotope effect of ∼2. These experimental results provide useful information about PCET in specific systems. Due to the limited number of systems studied, however, these experimental results do not provide a general understanding of the fundamental principles of PCET.

In this paper, we apply a recently developed theoretical formulation of PCET[15−18] to a series of model systems to determine the effects of solute and solvent properties on the rates, mechanisms, and kinetic isotope effects for PCET reactions. This systematic study elucidates some of the fundamental principles of PCET. In addition, this investigation aids in the interpretation of the available experimental results on model systems. Most importantly, this study provides predictions that can be tested experimentally.

The theoretical formulation in this paper is based on a multistate continuum theory, in which the solute is described with a multistate valence bond model, the solvent is represented as a dielectric continuum, and the transferring protons are treated

10.1021/jp001967s CCC: $19.00
Published on Web 00/00/0000 PAGE EST: 15

quantum mechanically.[15−18] (As discussed in ref 17, this theoretical formulation is distinct from the previous formulation of PCET by Cukier and co-workers.[9,19]) In our formulation, the mixed electronic/proton vibrational free energy surfaces are obtained as functions of two scalar solvent coordinates corresponding to proton and electron transfer. These free energy surfaces provide information about the mechanism of PCET. For example, in some cases only the electron transfers, while in other cases both the electron and the proton transfer either sequentially or concertedly. Recently, Soudackov and Hammes-Schiffer derived a rate expression for PCET in the limit of nonadiabatic electron transfer within the framework of this theoretical formulation.[17] Rate expressions in the limit of adiabatic electron transfer are also available.[18,27] The kinetic isotope effects can be calculated by replacing the transferring hydrogen with deuterium. This theory may be viewed as a multidimensional extension of standard Marcus theory for single electron transfer.

The basic model system in this paper consists of an electron donor and acceptor connected by a symmetric proton transfer interface represented by a protonated water dimer. We vary the following physical parameters in this model system: the electron donor−acceptor distance, the proton donor−acceptor distance, the energy differences between the electronic states, the coupling between the electronic states, the solute size, and the solvent polarity. The free energy surfaces, rates, and kinetic isotope effects are calculated for each model system. The analysis of these results leads to predictions of qualitative trends that can be tested experimentally.

An outline of this paper is as follows. Section II summarizes our theoretical formulation for PCET and describes the model system in this study. Section III presents the results, including a complete analysis of the dependence of the free energy surfaces, mechanisms, rates, and kinetic isotope effects on the solute and solvent properties. Section IV summarizes the general conclusions and predictions from this investigation of PCET reactions.

II. Theory and Model

A. Theory for PCET. Reference 15 presents the detailed derivation of a multistate continuum theory[20,21] for PCET reactions in solution. In this section, we briefly summarize this theory. The PCET system is represented by a four-state valence bond (VB) model[22] with electronic VB states defined as

$$\begin{aligned}
&(31a)\quad D_e^- - {}^+D_pH \cdots \cdots A_p - A_e\\
&(1b)\quad D_e^- - D_p \cdots \cdots HA_p^+ - A_e\\
&(2a)\quad D_e - {}^+D_pH \cdots \cdots A_p - A_e^-\\
&(2b)\quad D_e - D_p \cdots \cdots HA_p^+ - A_e^-
\end{aligned} \tag{1}$$

Here the symbols D_e and A_e represent a general electron donor and acceptor, D_p and A_p represent a general proton donor and acceptor, and H represents the transferring proton. The VB states are labeled as follows: *a* denotes that the proton is bonded to its donor while *b* denotes that the proton is bonded to its acceptor, and 1 denotes that the electron is localized on its donor while 2 denotes that the electron is localized on its acceptor. Thus, *a* and *b* indicate the proton transfer (PT) state, and 1 and 2 indicate the electron transfer (ET) state. The active electrons and transferring proton are treated quantum mechanically.

The solvent is represented as a dielectric continuum characterized by the electronic and inertial dielectric constants ϵ_∞ and ϵ_0, respectively. The Born−Oppenheimer approach is adopted for the separation of solvent and solute electronic time scales. In this approximation,[23] the solvent electrons are assumed to be infinitely fast on the time scale of the solute electrons. In this paper, electronic polarization refers to the solvent response assumed to be instantaneous, and inertial polarization refers to the non-instantaneous solvent response (e.g., nuclear reorientation and translation).

In this theory, the mixed electronic/proton vibrational free energy surfaces are obtained as functions of two scalar solvent coordinates z_p and z_e corresponding to the proton and electron transfer reactions, respectively. Each scalar solvent coordinate represents the difference in interaction energy of the two VB states involved in the charge transfer reaction with the inertial polarization field $\phi_{in}(\mathbf{r})$ of the solvent. Thus

$$\begin{aligned}
z_p &\equiv y'_{1b} = \int [\rho_{1b,1b}(\mathbf{r}) - \rho_{1a,1a}(\mathbf{r})]\phi_{in}(\mathbf{r})\, d\mathbf{r}\\
z_e &\equiv y'_{2a} = \int [\rho_{2a,2a}(\mathbf{r}) - \rho_{1a,1a}(\mathbf{r})]\phi_{in}(\mathbf{r})\, d\mathbf{r}
\end{aligned} \tag{2}$$

where $\rho_{ii}(\mathbf{r})$ is the total charge density of VB state *i*. These scalar solvent coordinates are analogous to the standard solvent coordinate used for the description of single charge transfer reactions.[24,25] As discussed in ref 15, the off-diagonal densities are neglected in this formulation.

The VB Hamiltonian matrix corresponding to the free energy is

$$\mathbf{H}(r_p,z_p,z_e) = S(r_p,z_p,z_e)\mathbf{I} + \mathbf{H}_o(r_p) + \begin{pmatrix} 0 & 0 & 0 & 0\\ 0 & z_p & 0 & 0\\ 0 & 0 & z_e & 0\\ 0 & 0 & 0 & z_p + z_e \end{pmatrix} \tag{3}$$

The first term is the transformed self-energy of the solvent inertial polarization and is expressed as

$$S(r_p,z_p,z_e) = \frac{1}{2}\sum_{i,j=1b,2a} \{[y'_i + t'_{1a,i}(r_p)][\mathbf{t}'_t(r_p)^{-1}]_{ij} \times [y'_j + t'_{1a,j}(r_p)]\} - \frac{1}{2}t'_{1a,1a}(r_p) \tag{4}$$

where the summation runs over valence bond states 1*b* and 2*a*, the truncated reorganization energy matrix $\mathbf{t}'_t$ has dimensions 2×2 corresponding to these two states, and $(z_p,z_e) \equiv (y'_{1b},y'_{2a})$. (The 1*a* state is eliminated through a coordinate transformation, and the 2*b* state is eliminated due to the linear dependency among the solvent coordinates.) The inertial reorganization energy matrix elements $t'_{ij}(q)$ are defined as

$$t'_{ij}(r_p) = -\int \nu_{jj}(\mathbf{r})[\hat{K}(\epsilon_0) - \hat{K}(\epsilon_\infty)]\nu_{ii}(\mathbf{r})\, d\mathbf{r} \tag{5}$$

where $\hat{K}(\epsilon)$ is the dielectric Green function[26] for the medium with dielectric constant ϵ and

$$\begin{aligned}
\nu_{1a,1a}(\mathbf{r}) &= \rho_{1a,1a}(\mathbf{r})\\
\nu_{ii}(\mathbf{r}) &= \rho_{ii}(\mathbf{r}) - \rho_{1a,1a}(\mathbf{r}) \qquad i = 1b,\ 2a,\ \text{or}\ 2b
\end{aligned} \tag{6}$$

The second term $\mathbf{H}_o(r_p)$ has matrix elements

$$(H_o)_{ij}(r_p) = (h_o)_{ij}(r_p) - \frac{1}{2}t_{ii}^{(\infty)}(r_p)\delta_{ij} \tag{7}$$

where h_o is the gas phase solute Hamiltonian and

$$t_{ij}^{(\infty)}(r_p) = -\int \rho_{jj}(\mathbf{r})\hat{K}(\epsilon_\infty)\rho_{ii}(\mathbf{r})\,d\mathbf{r} \quad (8)$$

is the electronic reorganization energy matrix element that accounts for the interaction of the solute with the electronic polarization of the solvent (within the Born−Oppenheimer approximation[23]). The third term in eq 3 represents the interaction of the solute with the inertial polarization of the solvent. Due to the coordinate transformation eliminating the 1*a* state, the transformed self-energy is the sum of the actual self-energy of the solvent inertial polarization and the interaction of the density of VB state 1*a* with the inertial polarization of the solvent. Since this interaction is included in the transformed self-energy, it is not included in the third term of eq 3.

Typically, PCET reactions involve electronically adiabatic PT since the proton donor and acceptor are strongly coupled due to hydrogen bonding. For electronically adiabatic PT reactions, the number of VB states can be reduced by eliminating the excited electronic states corresponding to the PT reactions. This is achieved by transforming the electronic VB basis set in eq 1 to another equivalent basis set in which the basis functions are the eigenvectors of the two 2 × 2 blocks of the matrix in eq 3 corresponding to the VB states 1*a*/1*b* and 2*a*/2*b*, respectively. For electronically adiabatic PT the higher excited electronic states for each block can be neglected, and the system can be described on the basis of the two remaining wave functions

$$\Psi_I(\mathbf{r}_e;r_p,z_p) = c_{1a}(r_p,z_p)\psi_{1a}(\mathbf{r}_e) + c_{1b}(r_p,z_p)\psi_{1b}(\mathbf{r}_e) \quad (9)$$

$$\Psi_{II}(\mathbf{r}_e;r_p,z_p) = c_{2a}(r_p,z_p)\psi_{2a}(\mathbf{r}_e) + c_{2b}(r_p,z_p)\psi_{2b}(\mathbf{r}_e) \quad (10)$$

with corresponding energies

$$E_I(r_p,z_p) = \frac{1}{2}\left\{(H_o)_{1a,1a}(r_p) + (H_o)_{1b,1b}(r_p) + z_p - \sqrt{[z_p + (H_o)_{1b,1b}(r_p) - (H_o)_{1a,1a}(r_p)]^2 + 4(H_o)_{1a,1b}(r_p)^2}\right\} \quad (11)$$

$$E_{II}(r_p,z_p) = \frac{1}{2}\left\{(H_o)_{2a,2a}(r_p) + (H_o)_{2b,2b}(r_p) + z_p - \sqrt{[z_p + (H_o)_{2b,2b}(r_p) - (H_o)_{2a,2a}(r_p)]^2 + 4(H_o)_{2a,2b}(r_p)^2}\right\} \quad (12)$$

Here, $\mathbf{r}_e$ denotes the electronic coordinates, and $\psi_i(\mathbf{r}_e)$ is the wave function associated with VB state *i*. In this notation, I and II correspond to ET states 1 and 2, respectively. The matrix corresponding to the free energy in this new basis set is

$$\mathbf{H}(r_p,z_p,z_e) = S(r_p,z_p,z_e)\mathbf{I} + \begin{pmatrix} E_I(r_p,z_p) & V(r_p,z_p) \\ V(r_p,z_p) & E_{II}(r_p,z_p) \end{pmatrix} + \begin{pmatrix} 0 & 0 \\ 0 & z_e \end{pmatrix} \quad (13)$$

where the coupling between the two electronic states Ψ_I and Ψ_{II} is

$$\begin{aligned} V(r_p,z_p) = {} & c_{1a}(r_p,z_p)c_{2a}(r_p,z_p)(h_o)_{1a,2a}(r_p) + \\ & c_{1b}(r_p,z_p)c_{2b}(r_p,z_p)(h_o)_{1b,2b}(r_p) + \\ & c_{1a}(r_p,z_p)c_{2b}(r_p,z_p)(h_o)_{1a,2b}(r_p) + \\ & c_{1b}(r_p,z_p)c_{2a}(r_p,z_p)(h_o)_{1b,2a}(r_p) \end{aligned} \quad (14)$$

The proton vibrational states can be calculated for each of the two new basis states by solving the one-dimensional Schrödinger equation

$$[T_p + H_{JJ}(r_p,z_p,z_e)]\phi_\mu^J(r_p;z_p,z_e) = \epsilon_\mu^J(z_p,z_e)\phi_\mu{}^J(r_p;z_p,z_e) \quad (15)$$

where T_p is the kinetic energy of the proton and $H_{JJ}(r_p,z_p,z_e)$ (J = I or II) is the diagonal element of the 2 × 2 matrix in eq 13. (As discussed in ref 17, the change in free energy $H_{JJ}(r_p,z_p,z_e)$ along the proton coordinate r_p is similar to the change in potential energy along r_p if the r_p dependence of the $v_{i,i}(\mathbf{r})$ is weak.) The resulting ET diabatic states are denoted $\Psi_I(\mathbf{r}_e;r_p,z_p)\phi_\mu^I(r_p;z_p,z_e)$ and $\Psi_{II}(\mathbf{r}_e;r_p,z_p)\phi_\nu^{II}(r_p;z_p,z_e)$ with corresponding free energies $\epsilon_\mu^I(z_p,z_e)$ and $\epsilon_\nu^{II}(z_p,z_e)$. The coupling between a pair of states Iμ and IIν is

$$V_{\mu\nu}(z_p) = \langle\phi_\mu^I|V(r_p,z_p)|\phi_\nu^{II}\rangle_p \quad (16)$$

where the subscript of the angular brackets indicates integration over r_p.

Many chemically and biologically relevant PCET reactions involve electronically nonadiabatic ET since the electron donor and acceptor are well-separated due to the presence of the proton transfer interface. Reference 17 presents a derivation of a rate expression for PCET in the regime of electronically nonadiabatic ET. In this limit, the Golden Rule may be used to calculate the rate of a transition from the two-dimensional free energy surfaces corresponding to the reactants (I) to those corresponding to the products (II). This derivation is based on two well-defined approximations: (1) the two-dimensional ET diabatic free energy surfaces $\epsilon_\mu^I(z_p,z_e)$ and $\epsilon_\nu^{II}(z_p,z_e)$ are assumed to be exact paraboloids with identical frequencies, and (2) the coupling $V_{\mu\nu}(z_p)$ between these surfaces is assumed to be constant for each pair of states for the relevant energies. As shown in this paper, these approximations are valid for a wide range of PCET systems.

The resulting rate expression in the limit of nonadiabatic ET (and in the absence of intramolecular solute modes) is

$$k = \frac{2\pi}{\hbar}\sum_\mu P_\mu^I \sum_\nu V_{\mu\nu}^2 (4\pi\lambda_{\mu\nu}k_BT)^{-1/2} \exp\left\{-\frac{(\Delta G_{\mu\nu}^\circ + \lambda_{\mu\nu})^2}{4\lambda_{\mu\nu}k_BT}\right\} \quad (17)$$

The equilibrium free energy difference is defined as

$$\Delta G_{\mu\nu}^\circ = \epsilon_\nu^{II}(\bar{z}_p^{II\nu},\bar{z}_e^{II\nu}) - \epsilon_\mu^I(\bar{z}_p^{I\mu},\bar{z}_e^{I\mu}) \quad (18)$$

and the reorganization energy is defined as

$$\lambda_{\mu\nu} = \epsilon_\mu^I(\bar{z}_p^{II\nu},\bar{z}_e^{II\nu}) - \epsilon_\mu^I(\bar{z}_p^{I\mu},\bar{z}_e^{I\mu}) \quad (19)$$

where $(\bar{z}_p^{I\mu},\bar{z}_e^{I\mu})$ and $(\bar{z}_p^{II\nu},\bar{z}_e^{II\nu})$ are the equilibrium solvent coordinates for states Iμ and IIν, respectively. Figure 1 depicts these quantities for a pair of paraboloids Iμ and IIν. The coupling $V_{\mu\nu}$ is defined in eq 16 and is evaluated at the solvent coordinate z_p corresponding to the intersection point along the straight-line reaction path connecting the minima of the two surfaces. The quantity P_μ^I is the Boltzmann distribution function for the reactant state μ.

In this paper, the ET diabatic free energy surfaces and the couplings were obtained with the alternative method described

$$\mathbf{h}_o(r_p) = \begin{pmatrix} U_{a,a}^{H_5O_2^+} + U_{1a,1a}^{Coul} & U_{a,b}^{H_5O_2^+} & V^{ET} & V^{EPT} \\ U_{b,a}^{H_5O_2^+} & U_{b,b}^{H_5O_2^+} + U_{1b,1b}^{Coul} & V^{EPT} & V^{ET} \\ V^{ET} & V^{EPT} & U_{a,a}^{H_5O_2^+} + U_{2a,2a}^{Coul} + \Delta E_{12} & U_{a,b}^{H_5O_2^+} \\ V^{EPT} & V^{ET} & U_{b,a}^{H_5O_2^+} & U_{b,b}^{H_5O_2^+} + U_{2b,2b}^{Coul} + \Delta E_{12} \end{pmatrix} \quad (20)$$

in refs 15 and 17. In the limit of electronically adiabatic PT, this alternative approach is exactly equivalent to the approach previously described. In this alternative approach, a set of N_{vib} proton vibrational states is calculated for each of the four VB states. The mixed electronic/proton vibrational states are expanded in terms of $4N_{vib}$ basis states, each composed of a product of an electronic VB state and an associated proton vibrational state. The ET diabatic states are obtained by diagonalizing the $4N_{vib} \times 4N_{vib}$ matrix obtained from eq 3 after setting $(h_o)_{ij}$ to zero if i and j represent different ET states. We verified that these two approaches are equivalent for the model systems in this paper.

B. Model PCET System. The model PCET system in this paper consists of electron donor and acceptor sites connected by a protonated water dimer, as depicted in Figure 2. The distance between the electron donor and acceptor is denoted R_{DA}, the distance between the proton donor and acceptor is denoted R_{OO}, and the coordinate of the proton relative to the center of the O−O bond is denoted r_p. For these studies, the positions of the non-transferring hydrogen atoms are determined from a minimized protonated dimer to ensure a symmetric proton transfer interface. For ET state 1 (or 2), the electron donor site has a charge of −1 (or 0), while the electron acceptor site has a charge of 0 (or −1). The PT states *a* and *b* are represented with the empirical valence bond model of Schmitt and Voth.[28] The two types of input required for our theoretical formulation are the gas phase matrix elements and the reorganization energy matrix elements. The remainder of this subsection will describe the calculations of these input quantities and will enumerate the parameters varied in our studies.

In our model, the gas phase matrix elements $(h_o)_{ij}$ are given by the matrix in eq 20, where the dependence of the diagonal matrix elements on r_p is omitted for notational simplicity. The 2×2 matrix $\mathbf{U}^{H_5O_2^+}(r_p)$ is the EVB matrix for a protonated water dimer given by Schmitt and Voth in ref 28. $U_{ii}^{Coul}(r_p)$ is the Coulomb interaction between the water dimer and the electron transfer donor and acceptor sites and can be expressed in terms of a sum over the PT sites (i.e., the 5 atoms of the protonated water dimer) and the ET sites (i.e., the ET donor and acceptor) as

$$U_{ii}^{Coul}(r_p) = \sum_{m}^{\text{ET sites}} \sum_{n}^{\text{PT sites}} \frac{q_m^i q_n^i}{R_{mn}} \quad (21)$$

Here, q_m^i and q_n^i represent the charges on the ET site m and the PT site n, respectively, for VB state i, and R_{mn} is the distance between these two sites. The parameter ΔE_{12} is the energy difference between the ET states 1 and 2 (and is assumed to be the same for PT states *a* and *b* and to be independent of r_p). The coupling V^{ET} between ET states 1 and 2 is given by

$$V^{ET} = V_0^{ET} \exp(-\beta R_{DA}/2) \quad (22)$$

where V_0^{ET} and β are approximated from previous calculations of electronic coupling for a water chain[29] and are set to 188.2 kcal/mol and 1.4 Å^{-1}, respectively. These values are assumed to be the same for PT states *a* and *b* and are not varied in our studies. The coupling V^{EPT} is one of the parameters varied in our studies. The couplings V^{ET} and V^{EPT} are assumed to be independent of r_p.

The reorganization energy matrix elements are calculated with a simple electrostatic ellipsoidal model developed by Kirkwood and Westheimer[30] and used recently by Cukier[19] for similar systems. In this model, the point charges representing the solute charge distribution for each VB state are placed on the main axis of an ellipsoidal cavity embedded in a dielectric continuum solvent characterized by the inertial (ϵ_0) and electronic (ϵ_∞)

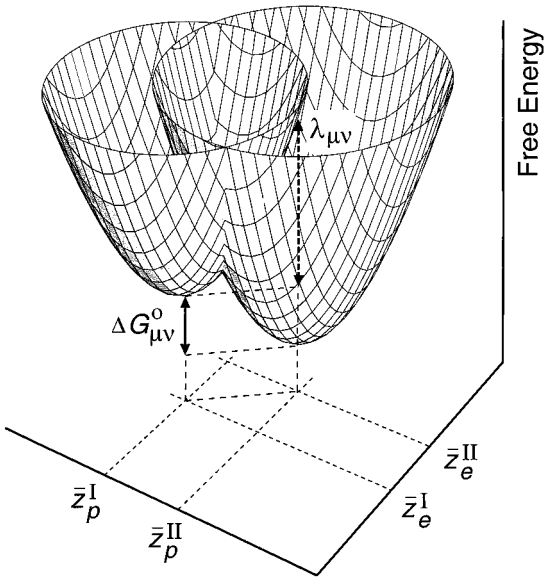

Figure 1. Schematic illustration of a pair of parabaloids Iμ and IIν as functions of the solvent coordinates z_p and z_e. The reorganization energy $\lambda_{\mu\nu}$ and the equilibrium free energy difference $\Delta G^{\circ}_{\mu\nu}$ are indicated.

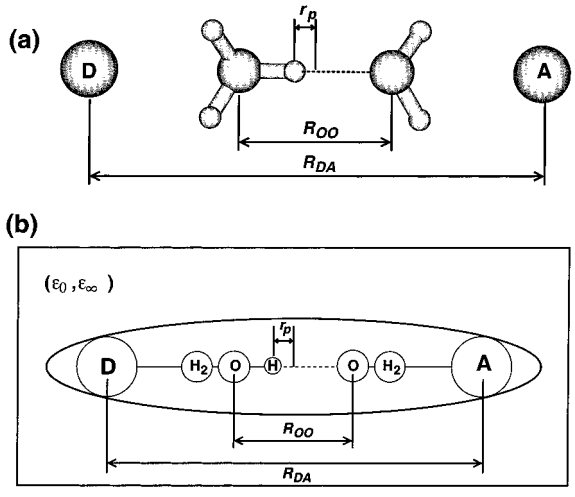

Figure 2. (a) PCET model used for the calculation of gas phase solute EVB Hamiltonian matrix elements. (b) Seven-site ellipsoidal model used for the calculation of solvent reorganization energies. R_{DA} is the electron donor−acceptor distance, R_{OO} is the proton donor−acceptor distance, and r_p is the proton coordinate.

dielectric constants. For this simple model, the electrostatic equations for the polarization potentials can be solved analytically, allowing the straightforward calculation of the solvation energies and reorganization energy matrix elements. In our model, the solute consists of seven sites on the main axis of the ellipsoidal cavity, as depicted in Figure 2*b*. Two of the sites represent the electron donor and acceptor, one of the sites represents the transferring proton, and the other four sites represent the two water molecules in the protonated water dimer. Each of these water molecules is described by two sites, where one site corresponds to the oxygen atom and the other site corresponds to the two hydrogen atoms. The charge of this latter site is the sum of the two hydrogen atoms, and the position of this site ensures the correct dipole moment for the water molecule.

The aim of our studies is to investigate the dependence of the rates, mechanisms, and kinetic isotope effects on the physical properties of the solute and solvent. The parameters varied in our studies are as follows:

1. R_{OO} is varied from 2.4 to 3.0 Å, therefore spanning the region where the proton potential energy curve is a single well to the region where the proton potential energy curve is a double well with a high barrier.

2. R_{DA} is varied from 10 to 20 Å. For $R_{DA} = 10$ Å, the electron transfer is in the adiabatic regime, but for $R_{DA} \geq 12$ Å, the electron transfer is in the nonadiabatic regime.

3. The energy difference ΔE_{12} between the ET states 1 and 2 is varied from exothermic (−20 kcal/mol) to endothermic (+20 kcal/mol).

4. The energy difference ΔE_{ab} between the PT states *a* and *b* is varied from exothermic (−5 kcal/mol) to endothermic (+5 kcal/mol). (Although not shown in eq 20, this parameter is added to the diagonal gas phase matrix elements corresponding to VB states 1*b* and 2*b*.) For simplicity, $\Delta E_{ab} = 0$ for all tables and figures presented in this paper.

5. The coupling V^{EPT} is varied between $0.1V^{ET}$ and $10V^{ET}$. For simplicity, $V^{EPT} = V^{ET}$ for all tables and figures in this paper.

6. The size of the ellipsoidal cavity is varied to investigate the effects of solute size. For simplicity, in all tables and figures presented in this paper, the ellipsoidal cavity in Figure 2b has a minor axis of 4.0 Å and a radius of 3.0 Å for the spheres representing the electron donor and acceptor. (The major axis was scaled according to R_{DA}.)

7. The inertial and electronic dielectric constants are varied to represent water ($\epsilon_0 = 78.4$ and $\epsilon_\infty = 1.77$) and methylene chloride ($\epsilon_0 = 8.93$ and $\epsilon_\infty = 2.02$) at 25 °C.[31]

III. Results and Discussion

This section presents a comprehensive analysis of our model system studies of PCET reactions. The first subsection describes the fundamental characteristics of the free energy surfaces and the dependence of these characteristics on the physical properties of the system. This subsection provides the groundwork for the next three subsections, which focus on the mechanisms, rates, and kinetic isotope effects, respectively.

A. Free Energy Surfaces. In the first part of this subsection, we discuss the fundamental principles of the free energy surfaces for PCET reactions. The general characteristics of the two-dimensional free energy surfaces and the associated proton potential energy curves and proton vibrational wave functions are presented. The limits of electronically and vibrationally adiabatic and nonadiabatic behavior are discussed. In the second part of this subsection, we predict the dependence of the characteristics of the free energy surfaces on the physical

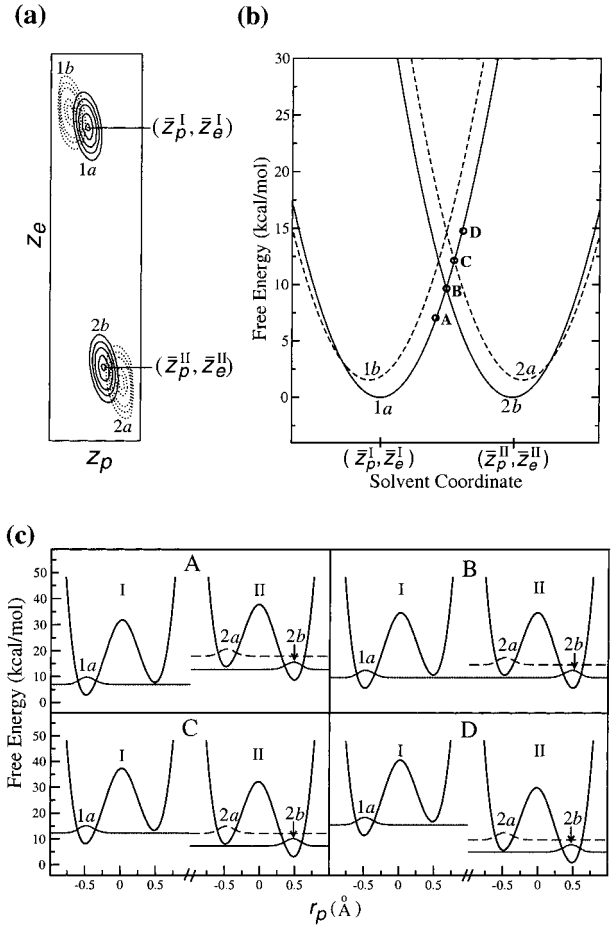

Figure 3. (a) Schematic illustration of two-dimensional ET diabatic mixed electronic/proton vibrational free energy surfaces as functions of the solvent coordinates z_p and z_e. Only two surfaces are shown for each ET diabatic state, and the lower and higher energy surfaces are shown with solid and dashed contour lines, respectively. The free energy surfaces are labeled according to the dominant VB state, and the minima of the lowest surfaces are labeled $(\bar{z}_p^{I},\bar{z}_e^{I})$ and $(\bar{z}_p^{II},\bar{z}_e^{II})$. (b) Slices of the free energy surfaces along the straight-line reaction path connecting the solvent coordinates $(\bar{z}_p^{I},\bar{z}_e^{I})$ and $(\bar{z}_p^{II},\bar{z}_e^{II})$ indicated in (a). (c) The reactant (I) and product (II) proton potential energy curves as functions of r_p at the solvent configurations corresponding to the points A, B, C, and D indicated on the lowest reactant ET diabatic surface in (b). The lowest reactant proton vibrational state and the lowest two product proton vibrational states are shown for each potential energy curve.

properties of the system and verify these predictions with our model system studies. In particular, we investigate the impact of altering the proton donor−acceptor distance, the electron donor−acceptor distance, the energy difference between the gas phase ET states, and the solvent polarity.

As previously discussed, for this model the free energy surfaces depend on two solvent variables, z_p and z_e, corresponding to proton and electron transfer, respectively. Figure 3 illustrates the fundamental physical principles underlying these surfaces. The two-dimensional ET diabatic surfaces $\epsilon_\mu^J(z_p,z_e)$ (J = I or II), defined in eq 15 are shown in the contour plots of Figure 3a and are labeled according to the dominant VB state. Note that the energy scale along the z_p axis is expanded by a factor of ∼4, so the disparity between the lengths of the z_p and z_e axes should be approximately 4 times greater. This disparity is due to the difference in reorganization energies for ET and PT. As previously mentioned, the reactants (I) and the products (II) correspond to ET states 1 and 2, respectively; the reactants are mixtures of the 1*a* and 1*b* VB states, while the products are mixtures of the 2*a* and 2*b* VB states. The PCET reaction can

be viewed as a transition from the surfaces corresponding to the reactants (I) to the surfaces corresponding to the products (II). Figure 3a shows that the minima of the ET diabatic surfaces within the set of reactants (or products) vary due to different weightings of the *a* and *b* PT states.

In this paper, for purposes of analysis, we depict slices of the two-dimensional ET diabatic surfaces along a straight-line reaction path connecting the lowest minima for the reactants (I) and the products (II). For example, the slices in Figure 3b were obtained from the straight-line reaction path connecting points ($\bar{z}_p^I$,$\bar{z}_e^I$) and ($\bar{z}_p^{II}$,$\bar{z}_e^{II}$) labeled in Figure 3a. For the remainder of the paper, we will show only the lowest energy reactant ET diabatic surface since for most of the systems studied, the Boltzmann population of the lowest reactant state is nearly unity (i.e., $P_1^I = 1$ in eq 17) at 25 °C. The free energy surfaces in Figure 3 are labeled according to the dominant VB state. For the model systems in this paper, the lowest reactant ET diabatic surface is dominated by the 1*a* VB state. A transition from this 1*a* reactant surface to a product ET diabatic surface dominated by the 2*a* VB state represents the ET mechanism (i.e., only the electron is transferred), and a transition from this 1*a* reactant surface to a product ET diabatic surface dominated by the 2*b* VB state represents the EPT mechanism (i.e., both the electron and the proton are transferred).

To gain more physical insight, we also investigate the proton potential energy curves $H_{JJ}(r_p,z_p,z_e)$ (J = I or II), defined in eq 13. Figure 3c depicts the reactant (I) and product (II) proton potential energy curves as functions of r_p at the four different solvent coordinates corresponding to points A, B, C, and D on the reactant ET diabatic surface in Figure 3b. The proton vibrational wave functions localized in the *a* well (near the proton donor) are associated with ET diabatic surfaces dominated by PT state *a*, and the proton vibrational wave functions localized in the *b* well (near the proton acceptor) are associated with ET diabatic surfaces dominated by PT state *b*. The proton vibrational wave functions delocalized above the proton transfer barrier are mixtures of PT states *a* and *b*. (No delocalized vibrational wave functions are shown in Figure 3c.) For the symmetric model systems in this paper, the *a* well is lower than the *b* well in the proton potential energy curves for the reactant (I), and the reverse is true for the product (II). This relation arises from the electron−proton Coulomb interaction, which lowers the energy when the electron and the proton are both on their donors or both on their acceptors.

Due to the coupling between the solvent and the solute, the proton potential energy curves depend strongly on the solvent coordinates. Figure 3c includes only the lowest energy reactant proton vibrational state (labeled according to the dominant VB state 1*a*) and the two lowest product proton vibrational states (labeled according to the dominant VB states 2*b* and 2*a*). The energy of each proton vibrational state shown in Figure 3c corresponds to the energy of the ET diabatic surfaces in Figure 3b at the specified solvent coordinates. Panels b and c of Figure 3 both indicate that, as the solvent coordinates change from A to D, the energy of the reactant ET diabatic state increases, while the energies of the product ET diabatic states decrease. These figures also illustrate that the lowest reactant state is lower in energy than the two lowest product states for the solvent coordinates associated with A, while the lowest reactant state is higher in energy than the two lowest product states for the solvent coordinates associated with D. Furthermore, panels b and c of Figure 3 show that for each intersection point of the reactant and product ET diabatic surfaces, the lowest proton vibrational state for the reactant (I) is degenerate with one of the proton vibrational states for the product (II). For the solvent coordinates associated with B, the lowest reactant state (1*a*) is degenerate with the lowest product state (2*b*), while for the solvent coordinates associated with C, the lowest reactant state is degenerate with the second product state (2*a*).

PCET reactions span a wide range of electronically adiabatic and nonadiabatic behaviors. We found that our model systems involve only electronically adiabatic PT reactions (i.e., $U_{a,b}^{H_5O_2^+}$ is much larger than the thermal energy k_BT), allowing us to reduce the four-state VB model to the two-state model described in section II. The ET and EPT reactions are electronically adiabatic if the coupling $V_{\mu\nu} \gg k_BT$, and they are electronically nonadiabatic if the coupling $V_{\mu\nu} \ll k_BT$. As shown in eq 16, the effective coupling $V_{\mu\nu}$ depends on the couplings V^{ET} and V^{EPT} between the VB states as well as the overlap of the reactant and product proton vibrational wave functions. Since the ET mechanism corresponds to the transition from a reactant 1*a* state to a product 2*a* state, the reactant and product vibrational wave functions are both localized in the *a* well of the proton potential energy curve and may have significant overlap. In contrast, the EPT mechanism corresponds to a transition from a reactant 1*a* state to a product 2*b* state, so the reactant and product vibrational wave functions are localized in different wells and have very small overlap. This difference in overlap for ET and EPT is illustrated in Figure 3c, where the overlap between the reactant 1*a* proton vibrational wave function and the product 2*a* proton vibrational wave function is nearly unity, while the overlap tween the reactant 1*a* proton vibrational wave function and the product 2*b* proton vibrational wave function is nearly zero. As a result of the small overlap of the reactant 1*a* and product 2*b* vibrational wave functions, the EPT mechanism is typically electronically nonadiabatic even when the ET mechanism is electronically adiabatic (i.e., even for small electron donor−acceptor distances). Thus, for reactions dominated by the EPT mechanism, the nonadiabatic rate expression in eq 17 is applicable even in the limit of electronically adiabatic ET. For reactions dominated by the electronically adiabatic ET mechanism, the standard rate expressions for adiabatic ET may be implemented.[27] For reactions involving both electronically nonadiabatic EPT and electronically adiabatic ET, a different rate expression must be derived. This paper will focus on the limit in which both ET and EPT are electronically nonadiabatic.

In addition to *electronically* adiabatic or nonadiabatic charge transfer reactions, the PT reaction may be *vibrationally* adiabatic or nonadiabatic. This issue arises if the proton vibrational states become degenerate within the set of reactant or product states for relevant energies. For small proton donor−acceptor distances (i.e., R_{OO} = 2.4 Å), this issue does not arise since the proton potential is a single well. For larger proton donor−acceptor distances, however, this issue becomes important due to the double well character of the proton potential. Panels a and b of Figure 4 depict the free energy slices for two model systems with R_{OO} = 2.8 and 3.0 Å, respectively. These figures indicate that for both models, the dominant VB states for two product ET diabatic surfaces are interchanged for solvent coordinates between the intersection of the reactant and product ET diabatic free energy surfaces and the minima of the relevant ET diabatic product surfaces. Figure 4c shows the product proton potential energy curves for the model system with R_{OO} = 3.0 Å for solvent coordinates before, at, and after the avoided crossing of the product states. These proton potential energy curves illustrate that at the avoided crossing, the second and third product proton vibrational states are nearly degenerate. Prior to the crossing, the third product state is localized in the *a* well

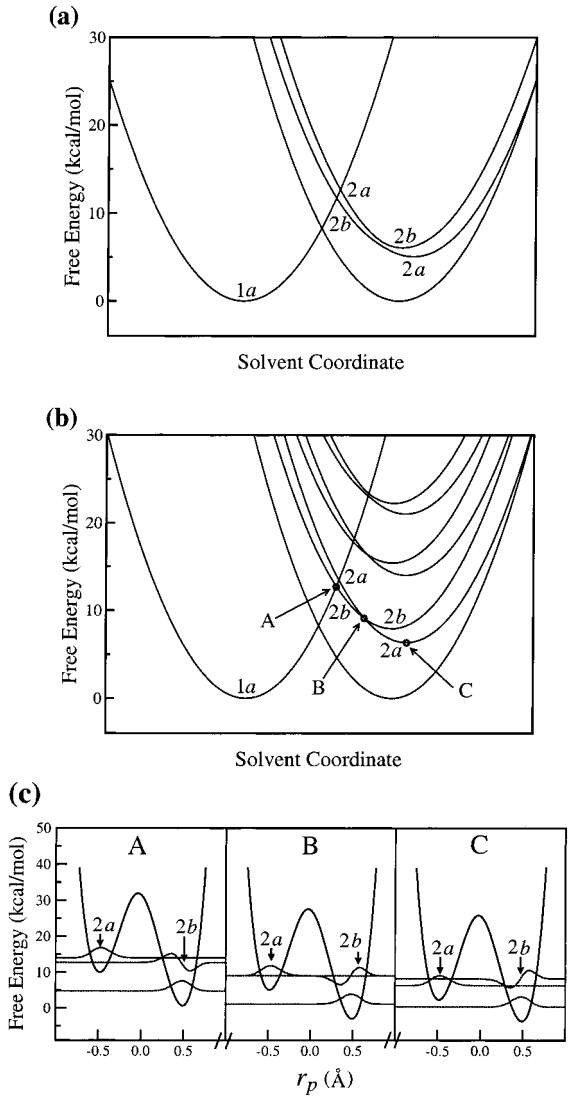

Figure 4. Slices of the ET diabatic free energy surfaces along the straight-line reaction path for a model system with (a) $R_{DA} = 13$ Å and $R_{OO} = 2.8$ Å (predominantly vibrationally adiabatic) and (b) $R_{DA} = 14$ Å and $R_{OO} = 3.0$ Å (vibrationally nonadiabatic). For both model systems, $\Delta E_{12} = 0$, and the solvent is water. The lowest reactant and the second and third product ET diabatic surfaces are labeled according to the dominant VB state. (c) The product proton potential energy curves at the solvent coordinates corresponding to A, B, and C indicated on the free energy surfaces in (b). The three lowest product proton vibrational states are shown for each potential energy curve, and the second and third ones are labeled according to the dominant VB state. Note that at the vibrationally nonadiabatic crossing, a pair of product proton vibrational states becomes degenerate, leading to a change in the dominant VB state for the corresponding ET diabatic free energy surfaces.

and the second product state is localized in the *b* well, and after the crossing, the localization of these states is interchanged. The tunnel splittings for the proton potential energy curves correspond to the splittings of the product ET diabatic surfaces at the avoided crossings. The tunnel splitting is significantly larger for Figure 4a than for Figure 4b due to a substantially lower proton transfer barrier for $R_{OO} = 2.8$ Å than for $R_{OO} = 3.0$ Å.

Thus, panels a and b of Figure 4 represent vibrationally adiabatic PT and vibrationally nonadiabatic PT, respectively, for the second and third product states at 25 °C. As a result, the two models represent qualitatively different mechanisms resulting from motion along the solvent reaction coordinate. Neglecting the lowest product state, Figure 4a represents two sequential reactions resulting in EPT and ET: in the first reaction, EPT occurs at the intersection between the reactant and the second product states, followed by vibrationally adiabatic PT when the relevant product state changes from 2*b* to 2*a*; in the second reaction, ET occurs at the intersection between the reactant and the third product states, followed by vibrationally adiabatic PT when the relevant product state changes from 2*a* to 2*b*. In contrast, Figure 4b represents both concerted EPT (transition from 1*a* to 2*b*) and ET (transition from 1*a* to 2*a*) reactions, followed by a vibrationally nonadiabatic crossing of the second and third product ET diabatic free energy surfaces. For the model system in Figure 4b, the fourth and fifth product states also exhibit a vibrationally nonadiabatic crossing, while the sixth and seventh product states are vibrationally adiabatic. The increase of the vibrational adiabaticity for higher states is due to the larger tunnel splittings (i.e., larger couplings) for states closer to the top of the proton transfer barrier. The rate expression in eq 17 may be applied to systems that are either vibrationally adiabatic or vibrationally nonadiabatic as long as the surfaces are still approximate paraboloids and the product states are correctly followed after the transition, according to the vibrationally adiabatic or nonadiabatic limits. On the other hand, the rate expression must be extended for situations between the vibrationally adiabatic and nonadiabatic limits.

The fundamental principles of PCET free energy surfaces discussed so far provide the foundation for our systematic investigation of the dependence of the free energy surfaces on the physical properties of the solute and the solvent. Our results are summarized in Figures 5 and 6. Figure 5a depicts the free energy slices for a typical set of parameters, and panels b−f of Figure 5 illustrate the effects of specific physical properties. The ET diabatic free energy surfaces are labeled according to the dominant VB states (and are not labeled in the absence of a clearly dominant VB state). In order to elucidate the effects of these physical properties, Figure 6 depicts proton potential energy curves at the minimum of the lowest product ET diabatic surface for a series of R_{OO} and R_{DA} values.

Increasing R_{OO} increases the proton transfer barrier and thus leads to a larger number of localized vibrational states. This phenomenon is confirmed by comparing panels a and b of Figure 5, which illustrate that increasing R_{OO} from 2.7 to 3.0 Å leads to a larger number of ET diabatic states dominated by either PT state *a* or PT state *b* (as opposed to a mixture of both *a* and *b*). For $R_{OO} = 2.4$ Å, the proton potential energy curve is a single well, so none of the states are localized near the proton donor or acceptor. Figure 6 shows that for larger R_{OO} distances, the proton potential energy curves are double well potentials, and the number of localized states increases with increasing R_{OO}. In addition, as shown in Figure 4, values of R_{OO} leading to double well potentials allow degeneracies of the proton vibrational states within each double well potential (i.e., within the set of reactant or product ET diabatic states). The resulting curve crossings within the set of reactant or product ET diabatic states are vibrationally nonadiabatic for large R_{OO} and are vibrationally adiabatic for smaller R_{OO}.

Increasing R_{DA} decreases the electron−proton Coulomb interaction and thus decreases the asymmetry of the proton potential energy curves. This trend is clearly illustrated by the proton potential energy curves in Figure 6. For very small R_{DA} distances, the asymmetry of the proton potential energy curve is so great that no product proton vibrational states are localized in the *a* well. For larger R_{DA} distances, this asymmetry decreases and thus allows a product proton vibrational state to be localized in the *a* well. As R_{DA} increases, the *a* well becomes lower in

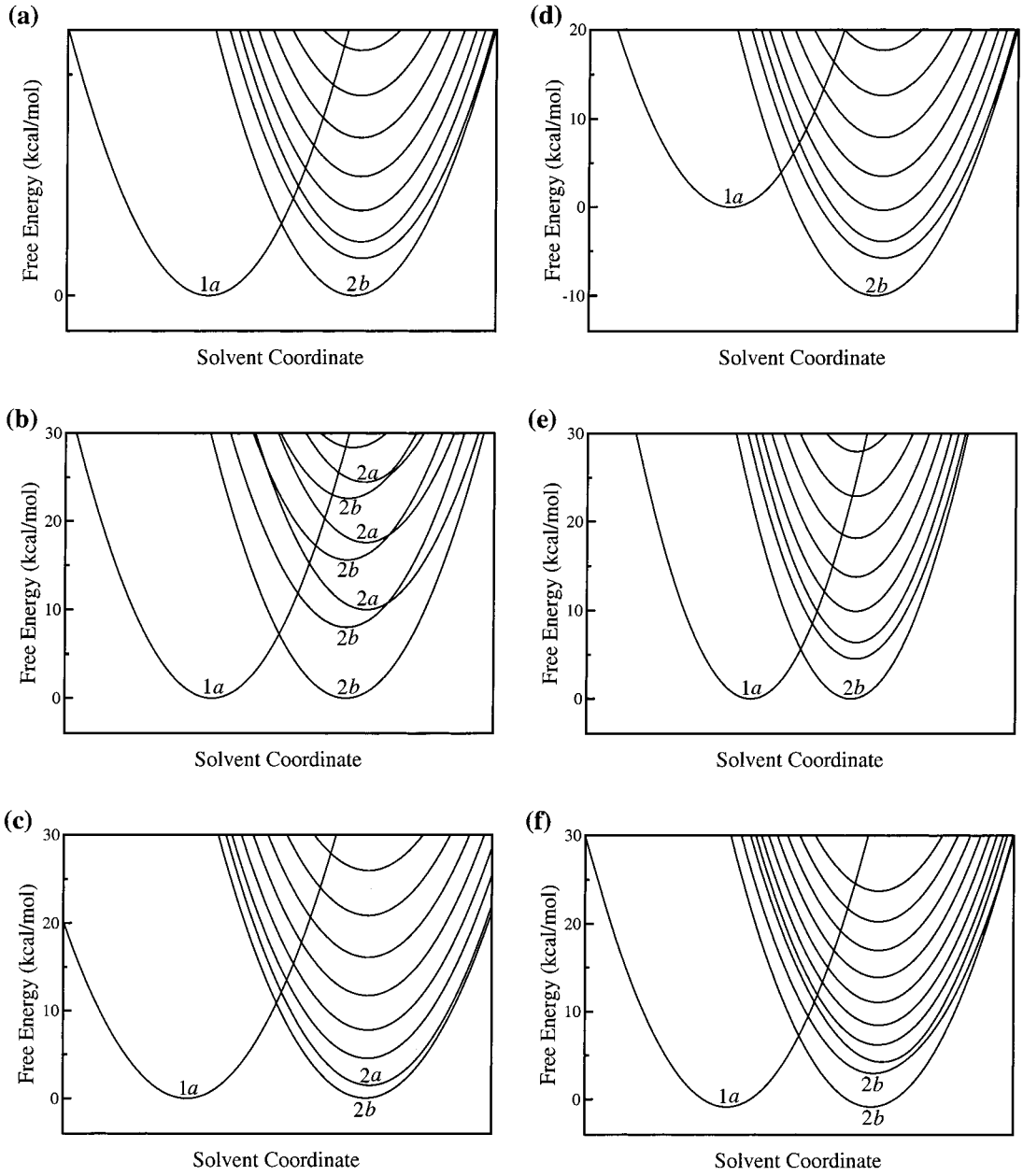

Figure 5. Slices of the free energy surfaces in water along a straight-line reaction path for a model system with (a) $R_{OO} = 2.7$ Å, $R_{DA} = 12$ Å, $\Delta E_{12} = 0$, (b) $R_{OO} = 3.0$ Å, $R_{DA} = 12$ Å, $\Delta E_{12} = 0$, (c) $R_{OO} = 2.7$ Å, $R_{DA} = 20$ Å, $\Delta E_{12} = 0$, (d) $R_{OO} = 2.7$ Å, $R_{DA} = 12$ Å, $\Delta E_{12} = -10$ kcal/mol. (e) Same as in (a) but in methylene chloride. (f) Same as in (a) but with deuterium substituted for the transferring hydrogen.

energy, so the energy difference between the lowest proton vibrational states localized in the *a* and *b* wells decreases. As a result, as R_{DA} increases, the lowest product ET diabatic state dominated by 2*a* becomes closer in energy to the lowest product ET diabatic state dominated by 2*b*. This trend is confirmed by a comparison of the ET diabatic surfaces in panels a and c of Figure 5, which show that increasing R_{DA} from 12 to 20 Å for $R_{OO} = 2.7$ Å changes the character of the second product ET diabatic state from delocalized to 2*a*. Comparison of Figures 4b ($R_{DA} = 14$ Å) and 5b ($R_{DA} = 12$ Å) for $R_{OO} = 2.8$ Å shows that increasing R_{DA} decreases the energy gap between the lowest 2*b* and 2*a* product states. This comparison also illustrates that the solvent coordinates corresponding to the curve crossings within the set of product ET diabatic states vary with R_{DA}.

Decreasing the energy difference ΔE_{12} between the gas phase ET states shifts the entire set of product ET diabatic surfaces down in energy by ΔE_{12}. (They are shifted up in energy if ΔE_{12} is increased.) This trend is illustrated by a comparison of panels a and d of Figure 5, which shows that decreasing ΔE_{12} from 0 to −10 kcal/mol shifts the product states down in energy. This model system is in the normal Marcus region, but when ΔE_{12} is sufficiently negative, the system will be in the inverted Marcus region (where the Marcus inverted region is defined as $-\Delta G^{\circ}_{\mu\nu} > \lambda_{\mu\nu}$).[32,33]

Finally, altering the polarity of the solvent affects both the reorganization energy matrix elements and the relative solvation energies of the VB states. Our analysis will focus on the changes in the reorganization energy matrix elements, which appear to be more important than the changes in the relative solvation energies for these model systems. In general, decreasing the solvent polarity decreases the reorganization energy matrix elements. According to standard Marcus theory for single ET reactions, as the reorganization energy decreases, the frequencies of the ET diabatic surfaces increase, and the difference between the solvent coordinates for the minima of the reactant and product ET diabatic surfaces decreases. As given in ref 17, an

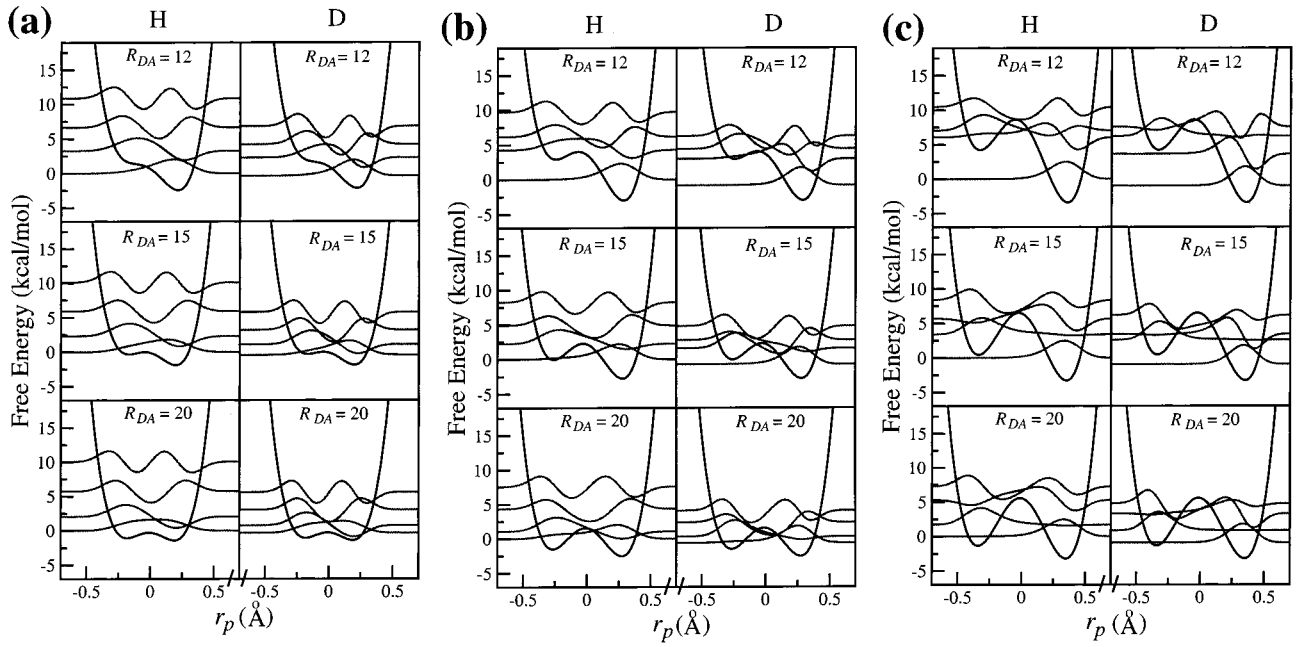

Figure 6. Product proton potential energy curves and the associated product proton vibrational wave functions at the solvent configurations corresponding to the minima of the lowest product ET diabatic free energy surfaces obtained with hydrogen for the values of R_{DA} indicated at the top of each frame and for (a) R_{OO} = 2.6 Å, (b) R_{OO} = 2.7 Å, and (c) R_{OO} = 2.8 Å. For all model systems, $\Delta E_{12} = 0$, and the solvent is water. Hydrogen wave functions are shown on the left, and deuterium wave functions are shown on the right.

analogous relation between reorganization energies and frequencies holds for PCET reactions, with the slight complication of the coupling term $t'_{1a,2b}$. For the model systems in this paper, we found that this coupling term does not alter the trend with solvent polarity. Thus, decreasing the solvent polarity increases the frequency and decreases the difference between the solvent coordinates of the reactant and product minima. These trends are illustrated by a comparison of panels a and e of Figure 5, which correspond to water (high polarity) and methylene chloride (lower polarity) solvents, respectively.

B. Mechanisms. In this subsection, we discuss the impact of the physical properties of the system on the mechanisms of PCET reactions. The two competing mechanisms, ET and EPT, are analyzed in terms of the rate expression given in eq 17. The general characteristics of the free energy surfaces and associated proton potential energy curves favoring each mechanism are presented. This analysis leads to predictions of the dependence of the mechanism on the proton donor−acceptor distance, the electron donor−acceptor distance, and the exothermicity of the gas phase ET. A detailed description of our model system studies is presented to verify these predictions. Table 1 provides the mechanisms for the various models, with both hydrogen and deuterium as the transferring nuclei in water and methylene chloride solvents. This subsection focuses on the mechanisms involving hydrogen transfer in aqueous solvent. At the end of this subsection, we describe the effects of solvent polarity on the mechanism. The effects of deuterium substitution are discussed in section III.D.

In this paper, the probabilities of EPT and ET are determined by calculating the percentage contribution P_ν of each product ET diabatic state ν to the rate and the contributions $p_{\nu a}$ and $p_{\nu b}$ of the a and b PT states, respectively, for each product ET diabatic state ν. The probability of EPT is defined as $P^{\mathrm{EPT}} = \sum_\nu^{\mathrm{states}} P_\nu p_{\nu b}$, and the probability of ET is defined as $P^{\mathrm{ET}} = \sum_\nu^{\mathrm{states}} P_\nu p_{\nu a}$. (For simplicity, these definitions approximate the reactant state as purely VB state 1a.) The mechanism is labeled "EPT" (or "ET") if P^{EPT} (or P^{ET}) is greater than 0.6. (For situations in which the relevant probability is within 0.02 of this cutoff, visual inspection of the wave functions was used to determine the mechanism.) The mechanism is labeled "N" if the reaction is neither ET nor EPT due to equal weightings $p_{\nu a}$ and $p_{\nu b}$ for the dominant product ET diabatic states. (This situation arises if the associated dominant product proton vibrational states are above the proton transfer barrier and thus are delocalized between the proton donor and acceptor.) The mechanism is labeled "B" if the reaction is both ET and EPT due to equal weighting P_ν but unequal weightings $p_{\nu a}$ and $p_{\nu b}$ for the dominant product ET diabatic states. (This situation arises if the dominant associated product proton vibrational states are below the proton transfer barrier and thus are localized in the a or b well of the proton potential energy curve, but the dominant product states are localized in different wells.)

The rate expression in eq 17 indicates that the rate increases with increasing coupling $V_{\mu\nu}$ and decreases with increasing free energy barrier $\Delta G^{\ddagger}_{\mu\nu}$. In other words, $k \propto V_{\mu\nu}^2 \exp(-\Delta G^{\ddagger}_{\mu\nu}/k_{\mathrm{B}}T)$, where $\Delta G^{\ddagger}_{\mu\nu} = (\Delta G^{\circ}_{\mu\nu} + \lambda_{\mu\nu})^2/4\lambda_{\mu\nu}$. As previously discussed, for proton donor−acceptor distances leading to a double well proton potential energy curve, the b well is always lower than the a well in the product proton potential energy curves for symmetric proton transfer interfaces due to the electron−proton Coulomb interaction. As a result, the lowest energy product ET diabatic state is dominated by 2b (corresponding to EPT). If the ET diabatic product states are assumed to not cross for relevant energies, the free energy barrier should be lowest for the lowest energy product state. Thus, typically the free energy barrier contribution to the rate favors EPT for symmetric PT interfaces. On the other hand, the coupling $V_{\mu\nu}$ is greatly affected by the overlap of the proton vibrational wave functions, as shown by eq 16. For a reactant state that is dominated by 1a, the overlap will be greatest for product states that are dominated by 2a, corresponding to ET. As a result, typically the coupling contribution to the rate favors ET.

The ET mechanism is possible only if one or more product proton vibrational states are localized in the a well of the product

TABLE 1: Values for the Rates, Kinetic Isotope Effects, and Mechanisms for a Series of PCET Model Systems[a]

			water				methylene chloride			
R_{OO}	R_{DA}	ΔE_{12}	rate	KIE	mech^{H+}	mech^{D+}	rate	KIE	mech^{H+}	mech^{D+}
2.6	12	−20	0.15×10^{10}	1.72	EPT	N	0.41×10^{11}	1.31	EPT	N
		−10	0.87×10^{7}	2.64	EPT	EPT	0.76×10^{9}	2.21	EPT	EPT
		0	0.54×10^{4}	3.38	EPT	EPT	0.72×10^{6}	3.41	EPT	EPT
		10	0.34	4.05	EPT	EPT	0.25×10^{2}	4.38	EPT	EPT
		20	0.20×10^{-5}	4.35	EPT	EPT	0.29×10^{-4}	5.07	EPT	EPT
	15	−20	0.13×10^{8}	1.35	N	N	0.62×10^{9}	1.21	N	N
		−10	0.52×10^{5}	1.49	EPT	N	0.91×10^{7}	1.48	EPT	N
		0	0.29×10^{2}	1.60	EPT	N	0.77×10^{4}	1.73	EPT	EPT
		10	0.21×10^{-2}	1.71	EPT	EPT	0.35	1.96	EPT	EPT
		20	0.20×10^{-7}	1.82	EPT	EPT	0.81×10^{-6}	2.18	EPT	EPT
	20	−20	0.40×10^{4}	1.01	N	N	0.37×10^{6}	1.02	N	N
		−10	0.13×10^{2}	1.06	N	N	0.41×10^{4}	1.08	N	N
		0	0.69×10^{-2}	1.12	N	N	0.32×10	1.16	N	N
		10	0.57×10^{-6}	1.18	N	N	0.18×10^{-3}	1.24	N	N
		20	0.76×10^{-11}	1.23	N	N	0.68×10^{-9}	1.31	N	N
2.7	12	−20	0.48×10^{9}	1.57	N	N	0.18×10^{11}	1.27	N	N
		−10	0.14×10^{6}	2.36	EPT	N	0.12×10^{9}	2.17	EPT	N
		0	0.61×10^{3}	3.78	EPT	N	0.64×10^{5}	4.79	EPT	N
		10	0.31×10^{-1}	5.54	EPT	N	0.17×10	10.34	EPT	N
		20	0.15×10^{-6}	8.42	EPT	N	0.14×10^{-5}	17.58	EPT	EPT
	15	−20	0.63×10^{7}	1.22	B	EPT*	0.34×10^{9}	1.08	ET	EPT*
		−10	0.22×10^{5}	1.41	B	EPT*	0.33×10^{7}	1.29	B	EPT*
		0	0.11×10^{2}	1.51	B	EPT*	0.21×10^{4}	1.58	B	EPT*
		10	0.69×10^{-3}	1.78	B	ET	0.73×10^{-1}	2.15	B	ET
		20	0.56×10^{-8}	1.90	B	ET	0.13×10^{-6}	2.40	EPT	ET
	20	−20	0.40×10^{4}	1.06	B	ET	0.31×10^{6}	1.17	B	ET
		−10	0.13×10^{2}	1.03	B	ET	0.31×10^{4}	1.23	B	ET
		0	0.51×10^{-2}	1.17	B	ET	0.22×10	1.26	B	ET
		10	–	–	B	ET	–	–	B	ET
		20	–	–	B	ET	–	–	B	ET
2.8	12	−20	0.13×10^{9}	1.21	EPT*	EPT*	0.99×10^{10}	1.63	ET	EPT*
		−10	0.21×10^{6}	1.40	EPT*	EPT*	0.32×10^{8}	2.35	ET	EPT*
		0	0.41×10^{2}	1.82	EPT*	EPT*	0.48×10^{4}	2.91	B	EPT*
		10	–	–	EPT*	ET	0.33×10^{-1}	3.01	EPT	ET
		20	–	–	EPT*	ET	0.12×10^{-7}	4.08	EPT	ET
	15	−20	0.31×10^{7}	1.05	EPT*	ET	0.23×10^{9}	1.11	EPT*	ET
		−10	0.96×10^{4}	1.40	ET	ET	0.14×10^{7}	1.20	ET	ET
		0	0.35×10	1.83	ET	ET	0.58×10^{3}	1.51	ET	ET
		10	–	–	ET	ET	–	–	ET	ET
		20	–	–	ET	ET	–	–	ET	ET
	20	−20	0.46×10^{4}	1.04	ET	ET	0.22×10^{6}	1.06	ET	ET
		−10	0.14×10^{2}	1.06	ET	ET	0.20×10^{4}	1.22	ET	ET
		0	0.51×10^{-2}	1.08	ET	ET	0.13×10	1.51	ET	ET
		10	0.33×10^{-6}	1.10	ET	ET	–	–	ET	ET
		20	0.26×10^{-11}	1.13	ET	ET	–	–	ET	ET

[a] The rates are given in units of s^{-1} for systems with H, and the kinetic isotope effect is defined as the ratio of the rate with H to the rate with D. The mechanisms are given for systems with H and systems with D. The notation for the mechanisms is defined as follows: ET corresponds to electron transfer, EPT corresponds to electron and proton transfer, B corresponds to both ET and EPT, N corresponds to neither ET nor EPT (i.e., delocalized vibrational wave functions), and EPT* corresponds to ET followed by PT. The parameters R_{OO} and R_{DA} are the donor−acceptor distances for proton and electron transfer, respectively, and are given in Å. The parameter ΔE_{12} is the energy difference between ET states 1 and 2 (where negative values correspond to exothermic reactions) and is given in kcal/mol. The solvent is either water or methylene chloride. Absent entries indicate numerical difficulties due to the locations of avoided crossings. The temperature is 25 °C.

proton potential energy curve. The shape of the proton potential energy curve is influenced mainly by R_{OO}, which determines the proton transfer barrier, and R_{DA}, which determines the electron−proton Coulomb interaction and thus the asymmetry. For very small R_{OO} values, the proton transfer barrier is so low or nonexistent that the proton potential energy curve is a single well, and the product vibrational states are either localized near the proton acceptor due to the electron−proton Coulomb interaction (leading to EPT) or delocalized (leading to neither ET nor EPT). As R_{OO} increases, the proton transfer barrier increases, leading to the possibility of the localization of a product proton vibrational wave function in the *a* well. Similarly, for very small R_{DA} values, the electron−proton Coulomb interaction is so strong that the proton potential energy curve is a single well localized near the proton acceptor, leading to EPT. As R_{DA} increases, the electron−proton Coulomb interaction (and hence the asymmetry) decreases, leading to a double well proton potential energy curve and the possibility of the localization of a product proton vibrational wave function in the *a* well.

For systems with product proton vibrational wave functions localized in the *a* well, the mechanism is determined by competition between the coupling and the free energy barrier. The lowest energy product ET diabatic state dominated by 2*b* (corresponding to EPT) is favored by the lower free energy barrier, while the higher energy product ET diabatic states dominated by 2*a* (corresponding to ET) are favored by the larger coupling. For very endothermic reactions, the lower free energy barrier for EPT overrides the larger coupling for ET, leading to the EPT mechanism. Conversely, for very exothermic reactions, the larger coupling for ET overrides the lower free energy barrier for EPT, leading to the ET mechanism. Furthermore, when the overlap between vibrational wave functions localized in opposite wells of the proton potential energy is extremely small (i.e.,

for very large R_{OO}), the larger coupling for ET overrides the lower free energy barrier for EPT, so the mechanism is ET.

These trends are validated by our model system studies. Although not included in Table 1, the mechanism for R_{OO} = 2.4 Å is predominantly N (i.e., neither ET nor EPT) or EPT. When the proton donor−acceptor distance is so short, the proton potential energy curve is a single well (i.e., no barrier to proton transfer). For large R_{DA} values, the proton vibrational wave functions are delocalized between the *a* and *b* PT states, and the weightings $p_{\mu a}$ and $p_{\mu b}$ are nearly equal for all product states, leading to neither ET nor EPT. For small electron donor−acceptor distances (i.e., R_{DA}=12 Å), the single well becomes so asymmetric due to the electron−proton Coulomb interaction that the EPT mechanism dominates (with $P^{EPT} \cong 0.6$). In this case, EPT corresponds to the single well proton potential energy curve shifting from the proton donor to the proton acceptor side.

Table 1 indicates that for R_{OO} = 2.6 Å, the mechanism is EPT or N for all values of R_{DA}. This observation is explained by the proton potential energy curves in Figure 6a, which illustrate that the proton transfer barrier is nearly nonexistent for R_{OO} = 2.6 Å. For R_{DA} = 12 Å, the lowest proton vibrational state is localized in the *b* well (corresponding to EPT), and no states are localized in the *a* well. For R_{DA} = 20 Å, the asymmetry of the double well potential is decreased due to smaller electron−proton Coulomb interactions, leading to a significant delocalization of the lowest proton vibrational state (corresponding to N).

As shown in Table 1, for R_{OO} = 2.7 Å, the higher proton transfer barrier allows all four mechanisms: EPT, ET, N, and B. This variety of possible mechanisms can be understood by analyzing the proton potential energy curves in Figure 6b. For all R_{DA} values, the lowest proton vibrational state is localized in the *b* well and corresponds to EPT. As R_{DA} increases, the asymmetry decreases, allowing the second product proton vibrational state to become somewhat localized in the *a* well. In particular, for R_{DA} = 12 Å, the second proton vibrational state as well as all higher states are delocalized. For the very exothermic reaction, the delocalized proton vibrational states dominate (i.e., the larger coupling of the third state overrides the lower free energy barriers of the first two states), so the reaction is neither ET nor EPT. For the less exothermic or endothermic reactions, the lowest proton vibrational state localized in the *b* well dominates (i.e., the lower free energy barrier of the lowest state overrides the larger coupling of the higher states), so the reaction is EPT. For R_{DA} = 15 Å and R_{DA} = 20 Å, the second proton vibrational state is somewhat localized in the *a* well, and all higher states are delocalized. Since both of the two lowest proton vibrational states contribute to the rate, the reaction is both ET and EPT.

For R_{OO} = 2.8 Å, the even higher proton transfer barrier allows the product proton vibrational states to become nearly degenerate, leading to the possibility of a sequential reaction, as shown in Figure 4a. At this proton donor−acceptor distance, the reactions are primarily vibrationally adiabatic and thus result in sequential reactions of two types: (1) reactions involving first EPT and then PT (overall ET) and (2) reactions involving first ET and then PT (overall EPT). Typically, the first type of sequential reaction is much less favorable than the second type due to the significantly smaller coupling for EPT than for ET. In Table 1, ET followed by PT is denoted EPT*. (To avoid numerical difficulties for these types of sequential reactions, the free energy barriers were obtained from the intersections of the free energy surfaces rather than from the expressions involving the equilibrium free energy differences and the reorganization energies.)

The mechanisms of the model systems with R_{OO} = 2.8 Å depend on the electron donor−acceptor distance R_{DA} and the exothermicity of the ET reaction ΔE_{12}. As shown in Figure 6c, for R_{OO} = 2.8 Å and R_{DA} = 12 Å the lowest two proton vibrational states are localized in the *b* well, and the third state is localized primarily in the *a* well. The larger coupling of the third state overrides the lower free energy barriers of the first two states, leading to ET at the intersection of the reactant and product ET diabatic surfaces. For these model systems, however, an avoided crossing between the second and third product proton vibrational states occurs in the region between the intersection of the reactant and product ET diabatic surfaces and the minima of the product ET diabatic surfaces. Specifically, the second and third product states are localized in the *b* and *a* wells, respectively, at the intersection of the reactant and product ET diabatic surfaces but are localized in the *a* and *b* wells, respectively, at the minima of these product ET diabatic surfaces. Thus, the dominant reaction is ET followed by vibrationally adiabatic PT, resulting in an overall EPT mechanism.

For R_{OO} = 2.8 Å and R_{DA} = 15 Å, the mechanism is particularly sensitive to the exothermicity of the ET reaction. As shown in Figure 6c, for these model systems the lowest state is localized in the *b* well, the second lowest state is localized in the *a* well, and the third lowest state is localized in the *b* well again. For ΔE_{12} = −20 kcal/mol, the mechanism is the sequential EPT mechanism (i.e., ET followed by vibrationally adiabatic PT). For the other values of ΔE_{12}, the avoided crossing between the second and third product proton vibrational states is shifted to the reactant side of the intersection of the reactant and product ET diabatic surfaces, so it no longer impacts the mechanism. In this case, the straightforward ET mechanism dominates.

The mechanism for R_{OO} = 2.8 Å and R_{DA} = 20 Å is less sensitive to the exothermicity. For these model systems, the lowest state is localized in the *b* well, and the next lowest state is localized in the *a* well. The avoided crossing between the second and third product proton vibrational states is shifted to the far side of the minima of the product ET diabatic surfaces, so it does not impact the mechanism. In this case, the state localized in the *a* well is close enough in energy to the state localized in the *b* well that the larger coupling determines the dominant product state for all values of ΔE_{12} studied, and the mechanism is always ET. All these results elucidate the dependence of the mechanisms on R_{DA} and ΔE_{12} for these model systems with R_{OO} = 2.8 Å.

Although not shown in Table 1, for R_{OO} = 3.0 Å, the mechanism is always ET for the range of R_{DA} and ΔE_{12} studied. In this case, the proton potential energy curve is always a double well potential with at least one product proton vibrational wave function localized in the *a* well. Furthermore, the high proton transfer barrier leads to an extremely small overlap between the proton vibrational wave functions localized in the *a* and *b* wells and thus to very small coupling for EPT compared to ET. As a result, the product states with the larger couplings dominate, leading to the ET mechanism. (A subsequent PT reaction is unlikely due to vibrational nonadiabaticity, as shown in Figure 4b.) Also not shown in Table 1 is the observation that the contribution of the EPT mechanism increases as the coupling V^{EPT} increases and as ΔE_{ab} (the energy difference of the PT states) decreases.

As shown in Table 1, the mechanisms are qualitatively similar in methylene chloride and in water. A quantitative analysis of

P^{EPT} for the different solvents, however, indicates that the probability of the EPT mechanism is greater in methylene chloride than in water due to the lower solvent polarity of methylene chloride. Decreasing the solvent polarity decreases the reorganization energy for each product ET diabatic state (with respect to the lowest reactant ET diabatic state). Moreover, decreasing the solvent polarity decreases the differences in the reorganization energies for pairs of product ET diabatic states. For the model systems in this paper, decreasing both the overall reorganization energies and the differences in the reorganization energies increases the differences in the free energy barriers for pairs of product ET diabatic states. This increase in the difference in the free energy barriers favors the lower product states, hence leading to a higher probability of EPT (which corresponds to the lowest product state). Thus, decreasing the solvent polarity increases the probability of the EPT mechanism.

C. Rates. In this subsection, we discuss the dependence of the rates of PCET reactions on the physical properties of the solute and solvent. We focus on the limit of nonadiabatic ET, for which the rate expression in eq 17 is valid. First, we provide a framework for our analysis by describing the dependence of each quantity in the rate expression on the various physical properties of the system. Subsequently, we predict the impact of each physical property of the system on the overall rate and verify each prediction with an analysis of our model system studies. In this subsection we discuss only the rates for PCET systems involving hydrogen (rather than deuterium) transfer.

The nonadiabatic rate expression in eq 17 depends on three quantities. The first quantity is the equilibrium free energy difference $\Delta G^{\circ}_{\mu\nu}$ between pairs of ET diabatic free energy surfaces. This quantity is directly affected by the parameter ΔE_{12}, representing the energy difference between the gas phase ET states 1 and 2. As ΔE_{12} increases, $\Delta G^{\circ}_{\mu\nu}$ also increases for all pairs of states. In addition, $\Delta G^{\circ}_{\mu\nu}$ is impacted by R_{OO} and R_{DA} through the electron−proton Coulomb interaction and the solute solvation energy. (The solvation energy depends on R_{OO} and R_{DA} since these parameters determine the charge densities of the four VB states.) $\Delta G^{\circ}_{\mu\nu}$ is also affected by R_{OO} through interactions within the protonated water dimer. Finally, $\Delta G^{\circ}_{\mu\nu}$ is influenced by the solvent polarity, which affects the solvation energy for the solute. The second quantity in the rate expression is the reorganization energy $\lambda_{\mu\nu}$ between pairs of ET diabatic free energy surfaces. This quantity is influenced by R_{OO} and R_{DA} (since these parameters determine the charge densities of the four VB states), as well as by the solvent polarity. The third quantity in the rate expression is the coupling $V_{\mu\nu}$ between pairs of ET diabatic free energy surfaces. As indicated by eqs 14 and 16, this quantity is determined by the couplings V^{ET} and V^{EPT} and by the proton vibrational wave functions. Since R_{DA} determines V^{ET} (through eq 22), R_{DA} significantly impacts $V_{\mu\nu}$. Moreover, both R_{OO} and R_{DA} affect the coupling since they influence the coefficients in eq 14 and the proton vibrational wave functions. The remainder of this subsection will analyze the rates in Table 1 within this framework. Note that minor deviations from the trends result from numerical difficulties near avoided crossings.

As previously discussed, R_{OO} affects all three quantities in the rate expression. The impact of R_{OO} on $V_{\mu\nu}$ is mainly due to the effect on the overlap of the proton vibrational wave functions: increasing R_{OO} decreases this overlap and thus decreases $V_{\mu\nu}$. Note that R_{OO} also affects the densities of the four VB states and the relative energies of the four gas phase VB states (through the electron−proton Coulomb interaction and the interactions within the protonated water dimer), leading to complex changes in all three quantities in the rate expression. Despite these complexities, we found that for these model systems, the dominant effect of R_{OO} on the rates is due to the impact on the proton vibrational overlap, which in turn influences the coupling. This observation is confirmed by Table 1, which indicates that increasing R_{OO} decreases the rate.

R_{DA} also affects all three quantities in the rate expression. The impact of R_{DA} on $V_{\mu\nu}$ is mainly due to the effect on V^{ET}: increasing R_{DA} decreases V^{ET} and thus decreases $V_{\mu\nu}$. Since R_{DA} also affects the electron−proton Coulomb interaction and the densities of the four VB states, however, it leads to complex changes in all three quantities in the rate expression. Nevertheless, we found that for these model systems the dominant effect of R_{DA} on the rates is due to the impact on the coupling V^{ET}. This observation is confirmed by Table 1, which shows that increasing R_{DA} decreases the rate.

In addition, the polarity of the solvent impacts both $\Delta G^{\circ}_{\mu\nu}$ and $\lambda_{\mu\nu}$ in the rate expression. Decreasing the solvent polarity decreases $\lambda_{\mu\nu}$, leading to a lower barrier along the solvent coordinates and thus increasing the rate. Decreasing the solvent polarity also alters the relative solvation energies of the four VB states, leading to complex changes in $\Delta G^{\circ}_{\mu\nu}$. We found that the main impact of the solvent polarity is through the reorganization energy. This observation is validated by Table 1, which indicates that decreasing the solvent polarity increases the rate. Although not shown in Table 1, increasing the size of the electron donor and acceptor also increases the rate for the same physical reasons as decreasing the solvent polarity.

Table 1 also shows that the rate decreases as ΔE_{12} increases (in the normal Marcus region). This observation is consistent with the direct relation between ΔE_{12} and $\Delta G^{\circ}_{\mu\nu}$ previously discussed. In the inverted Marcus region, the rate will decrease as ΔE_{12} decreases. Although not shown in Table 1, we also found that the rate decreases as the coupling V^{EPT} decreases and as ΔE_{ab} increases. Note that for some of these model systems (i.e., those with very large ΔE_{12}), the rates are so slow that they would not be observable on a physically reasonable time scale. These nonphysical model systems are included only to illustrate the trends.

D. Kinetic Isotope Effects. In this subsection, we discuss the impact of the physical properties of a PCET system on the kinetic isotope effect (i.e., the ratio of the rate with hydrogen to the rate with deuterium). The effects of deuterium substitution are determined by changing the mass of the transferring nucleus for the calculation of the vibrational wave functions. In the first part of this subsection, we analyze the impact of deuterium substitution on the mechanisms and rates in terms of the quantities in the nonadiabatic rate expression given in eq 17. After this general discussion, we verify these fundamental predictions with our model system studies. In the latter part of this subsection, we investigate the dependence of the magnitude of the kinetic isotope effect on the physical properties of the system within the framework of our model system studies. This subsection concludes with an explanation of the unusually large kinetic isotope effects that are observed for some of the model systems.

Table 1 provides the kinetic isotope effects and the mechanisms observed with deuterium. As expected, we found that the zero point energy and the splittings between the vibrational states are smaller for deuterium than for hydrogen. As a result, more vibrational states may be localized in the *a* and *b* wells for deuterium, leading to a qualitatively different set of vibrational states. These differences are confirmed by comparing panels a and f of Figure 5, which illustrate that substitution of

deuterium for the transferring hydrogen allows the second state to be localized in the *b* well and decreases the splittings between the vibrational states. These phenomena are also illustrated in Figure 6. In some cases, these changes cause the mechanism and rate to be substantially different when deuterium is substituted for hydrogen.

The changes in mechanism upon substitution with deuterium may be analyzed in terms of the competition between the coupling and the free energy barrier. As previously discussed, for these model systems, the lowest energy product vibrational state is localized in the *b* well, leading to EPT. The possibility of a higher product vibrational state localized in the *a* well is greater for deuterium than for hydrogen due to the smaller zero point energy for deuterium. Moreover, the higher states localized in the *a* well (or delocalized if the proton transfer barrier is too low to allow localization in the *a* well) have lower free energy barriers for deuterium due to the smaller splittings between vibrational states. In addition, the coupling for EPT is much smaller for systems with deuterium than for systems with hydrogen, while the coupling for ET is similar for the two types of systems. As a result, for systems with deuterium, the larger coupling for ET is more likely to override the lower free energy barriers for EPT, leading to a higher contribution of the ET mechanism for systems with deuterium. As will be discussed below, we observed this phenomenon for our model systems.

The impact of deuterium substitution on the rate may be analyzed in terms of the three quantities in the nonadiabatic rate expression given in eq 17. The reorganization energies $\lambda_{\mu\nu}$ are affected since the solvent coordinates of the minima of the ET diabatic free energy surfaces are altered. We found the impact of this effect on the rates to be relatively insignificant. The equilibrium free energy differences $\Delta G^\circ_{\mu\nu}$ are affected by deuterium substitution due to the smaller splittings between the vibrational states for deuterium. The values of $\Delta G^\circ_{\mu\nu}$ for the lowest product vibrational states localized in the *a* and *b* wells are not altered significantly since the zero point energy is approximately the same in the reactant and product ET diabatic states. On the other hand, for all other product vibrational states, $\Delta G^\circ_{\mu\nu}$ will be lower for deuterium than for hydrogen due to the smaller splittings between the vibrational states of deuterium. This difference in equilibrium free energies could lead to an inverse kinetic isotope effect, although this was not observed for our model systems. The couplings $V_{\mu\nu}$ are affected by deuterium substitution since these couplings are averaged over different vibrational wave functions. In general, the overlap of vibrational wave functions in different wells (i.e., one localized in the *a* well and one localized in the *b* well) is smaller for deuterium than for hydrogen, leading to smaller couplings for EPT with deuterium than with hydrogen. In some cases, this difference in couplings leads to very large kinetic isotope effects, as observed in our model systems.

These fundamental principles concerning kinetic isotope effects for PCET reactions are validated by the results given in Table 1. For $R_{DA} = 2.6$ Å, three model systems exhibit a change from EPT for hydrogen to neither ET nor EPT (denoted N) for deuterium. As shown in Figure 6a, in this case the deuterium wave functions are qualitatively similar to the hydrogen vibrational wave functions. The ground state is localized in the *b* well, and the next lowest state is delocalized. The mechanism is determined by competition between the coupling (which favors N) and the free energy barrier (which favors EPT). For systems with deuterium, the coupling for EPT is significantly smaller, and the energy of the second product vibrational state is slightly lower in energy than for systems with hydrogen. As a result, the second product vibrational state is more likely to dominate for systems with deuterium, leading to more cases of the N mechanism (i.e., neither ET nor EPT).

For $R_{OO} = 2.7$ Å, substitution with deuterium leads to qualitatively different vibrational wave functions, as shown in Figure 6b. For $R_{DA} = 12$ Å and $\Delta E_{12} \geq -10$ kcal/mol, the hydrogen system is EPT, and the deuterium system is N. In the hydrogen system, the dominant product vibrational state is the lowest state, which is localized in the *b* well, whereas in the deuterium system, the dominant product vibrational state is the third state, which is fairly delocalized. For $R_{DA} = 15$ and 20 Å, the hydrogen system is both ET and EPT (denoted B), and the deuterium system is either ET followed by PT (denoted EPT*) or ET. In the hydrogen system, the dominant product vibrational states are the lowest two states, which are each localized in one of the wells, while in the deuterium system, the dominant product vibrational state at the intersection is the second state, which is localized in the *a* well. The EPT* mechanism is observed for the deuterium system if an avoided crossing occurs in the relevant region. These differences result from the smaller coupling for EPT and the smaller splittings between the vibrational states for deuterium.

The effect of deuterium substitution for $R_{OO} = 2.8$ Å is influenced by the avoided crossings of the product vibrational states. For both hydrogen and deuterium, the ET mechanism dominates at the intersection of the reactant and product ET diabatic surfaces. This phenomenon is due to the localization of a product vibrational state in the *a* well and the substantially larger coupling for this state than for the lower states localized in the *b* well. For some model systems, however, an avoided crossing between two product vibrational states is located between the intersection of the relevant reactant and product ET diabatic surfaces and the minima of the relevant product ET diabatic surfaces. These model systems exhibit the EPT* mechanism, where ET is followed by vibrationally adiabatic PT. Thus, the differences between the mechanisms (ET or EPT*) for hydrogen and deuterium are due mainly to the location of the avoided crossing between the product vibrational states. Note that for endothermic systems with $R_{DA} = 12$ Å in methylene chloride, the mechanism is EPT for hydrogen and ET for deuterium. This difference is due to the smaller coupling for EPT and the smaller splittings between the vibrational states for deuterium.

The magnitudes of the kinetic isotope effects in Table 1 exhibit several interesting trends. First, for fixed values of R_{OO} and R_{DA}, the kinetic isotope effect becomes larger as the reaction becomes more endothermic (i.e., as ΔE_{12} increases). Second, for fixed values of R_{OO} and ΔE_{12}, the kinetic isotope effect becomes larger as R_{DA} decreases. (Although not shown in Table 1, this trend is also validated by studies of model systems with $R_{DA} = 10$ Å.) Third, for fixed values of R_{OO} and R_{DA}, the kinetic isotope effect becomes larger as the solvent polarity decreases for $\Delta E_{12} \geq 0$. All three of these trends may be explained by the same fundamental principle: the kinetic isotope effect increases as the contribution of the EPT mechanism increases. (If the mechanism is pure ET, the kinetic isotope effect is nearly unity.) As ΔE_{12} increases (in the normal Marcus region) the contribution of EPT increases since the lower free energy barrier of the lowest state localized in the *b* well overrides the larger coupling of the higher states localized in the *a* well. As R_{DA} decreases, the contribution of EPT increases since the electron−proton Coulomb interaction increases, so the asymmetry of the proton potential energy curve increases. The increased asymmetry will raise the energy of the product

vibrational state localized in the *a* well and may even prevent any product vibrational states from being localized in the *a* well. As the solvent polarity decreases, the contribution of EPT increases since the difference in free energy barriers for the various product ET diabatic states increases, leading to a greater contribution of the lower product vibrational states localized in the *b* well. This influence of the solvent polarity on the kinetic isotope effect is less significant for exothermic reactions in which the larger coupling of the ET states almost completely overrides the lower free energy barrier of the EPT states. Although not shown in Table 1, increasing the size of the electron donor and acceptor also increases the kinetic isotope effect for the same physical reasons as decreasing the solvent polarity. In addition, we observed that increasing the coupling V^{EPT} and decreasing ΔE_{ab} increases the kinetic isotope effect due to increased contribution of the EPT mechanism.

The dependence of the kinetic isotope effects on R_{OO} is not straightforward since it involves two opposing factors. Increasing R_{OO} decreases the kinetic isotope effect due to the decreased contribution of the EPT mechanism, but it also increases the kinetic isotope effect due to a larger ratio of the hydrogen-to-deuterium couplings. As a result, the kinetic isotope effects are largest for intermediate proton donor−acceptor distances. The decrease in the contribution of the EPT mechanism as R_{OO} increases is due to the smaller overlap of the reactant and product vibrational wave functions involved in EPT. The increase in the ratio of the hydrogen-to-deuterium couplings as R_{OO} increases can also be explained in terms of the overlap of the reactant and product vibrational wave functions. When the EPT mechanism dominates, the coupling is averaged over the product of two vibrational wave functions localized in different wells of the proton potential energy curve. The overlap of these two vibrational wave functions is significantly smaller for deuterium than for hydrogen. Moreover, the ratio of the overlap of the reactant and product vibrational wave functions for hydrogen to that for deuterium increases as the distance between the centers of the reactant and product wave functions increases. Hence, the ratio of the hydrogen-to-deuterium couplings increases as R_{OO} increases. Similarly, decreasing R_{DA} increases the localization of and the distance between the reactant and product proton vibrational wave functions.

In some cases, the kinetic isotope effects are quite large (i.e., >5) for our model systems. One explanation for the large kinetic isotope effects is that the probability of EPT is larger for hydrogen than for deuterium. Although this factor contributes to the large kinetic isotope effects, we found that the most important factor is the coupling term in the rate expression. One significant difference between EPT reactions and single PT reactions is that typically the vibrational wave functions for EPT reactions are more localized near the proton donor or acceptor and thus have much smaller overlaps between reactant and product wave functions. The highly localized nature of the vibrational wave functions in EPT reactions is due to the asymmetry of the proton potential energy curve induced by the electron−proton Coulomb interaction. This asymmetry can be viewed as producing a very high and wide effective barrier to proton transfer, leading to large kinetic isotope effects.

IV. Concluding Remarks

In this paper, we presented a comprehensive theoretical study of model systems aimed at predicting the effects of solute and solvent properties on the rates, mechanisms, and kinetic isotope effects for PCET reactions. These studies are based on a multistate continuum theory, in which the solute is described with a multistate valence bond model, the solvent is represented as a dielectric continuum, and the active electrons and transferring protons are treated quantum mechanically. In this theoretical formulation, the reactant and product ET diabatic free energy surfaces are obtained as functions of two solvent coordinates corresponding to proton and electron transfer. PCET reactions are viewed as transitions between the reactant and product ET diabatic free energy surfaces. The rates and kinetic isotope effects for PCET are calculated with a recently derived rate expression for nonadiabatic PCET. (Even in the limit of electronically adiabatic ET, the EPT mechanism is typically electronically nonadiabatic due to the small overlap of the reactant and product proton vibrational wave functions.) The detailed mechanisms (i.e., whether the reactions are ET or EPT, and if EPT, whether they are concerted or sequential) are determined by analyzing the character of the dominant product ET diabatic free energy surfaces.

The mechanism for PCET reactions depends strongly on the proton donor−acceptor distance. We found that there are four distinct regimes of proton donor−acceptor distances. The first regime corresponds to proton donor−acceptor distances that are so small that all proton vibrational wave functions are delocalized between the proton donor and acceptor such that the EPT mechanism is not well-defined. The second regime corresponds to proton donor−acceptor distances that are large enough to have at least one product proton vibrational wave function localized near the proton acceptor but small enough to prevent any product proton vibrational wave functions from being localized near the proton donor. In this case, the EPT mechanism will dominate and will always be concerted. The third regime corresponds to intermediate proton donor−acceptor distances with a high enough proton transfer barrier to allow at least one product proton vibrational wave function to be localized near the proton donor. In this case, the EPT mechanism will compete with the ET mechanism and may be concerted or sequential. Typically for sequential EPT reactions, the ET step precedes the PT step. The fourth regime corresponds to large proton donor−acceptor distances with such a high proton transfer barrier that the EPT mechanism is no longer possible due to small coupling (i.e., the ET mechanism is dominant).

Our results predict that the probability of the EPT mechanism will increase as (1) the electron donor−acceptor distance is decreased, (2) the proton donor−acceptor distance is decreased (until the distance is so short that the proton is delocalized), (3) the PT reaction becomes more exothermic (or less endothermic), (4) the ET reaction becomes more endothermic (or less exothermic) in the normal Marcus regime, (5) the temperature decreases, (6) the solvent polarity decreases, and (7) the size of the electron donor and acceptor increases.

All these factors impact the competition between the couplings (which typically favor ET) and the free energy barriers (which typically favor EPT). Decreasing the electron−donor acceptor distance increases the electron−proton Coulomb interaction, which decreases the equilibrium free energy difference (and hence the free energy barrier) for EPT relative to ET. Decreasing the proton donor−acceptor distance increases the overlap (and hence the coupling) between reactant and product proton vibrational wave functions involved in EPT. Increasing the exothermicity of the PT reaction decreases the equilibrium free energy difference (and hence the relative free energy barrier) for EPT relative to ET. Increasing the endothermicity of the ET reaction (or decreasing the temperature) in the normal Marcus region decreases the rate of both ET and EPT but increases the probability of EPT since the lower free energy barrier for EPT overrides the larger coupling for ET.

Decreasing the solvent polarity and the size of the electron donor and acceptor alters the reorganization energies in a way that increases the free energy barrier for ET relative to that for EPT.

The rate of the EPT mechanism will also increase as the properties of the system are altered in the ways previously enumerated above, with the exception of the exothermicity of the ET reaction and the temperature. The rate of the EPT mechanism will increase while the probability of the EPT mechanism will decrease as the ET reaction becomes more exothermic in the normal Marcus region. In the inverted Marcus region, the probability of the EPT mechanism will increase but the rate of EPT will decrease as the ET reaction becomes more exothermic. These trends are due to the domination of the EPT mechanism over the ET mechanism for higher overall free energy barriers since the lower free energy barrier for EPT overrides the larger coupling for ET. On the other hand, the rates of both ET and EPT clearly decrease for higher free energy barriers. For similar reasons, the probability of EPT increases but the rate of EPT decreases as the temperature is decreased. At lower temperatures, the mechanism with the lower free energy barrier dominates, favoring EPT over ET in the normal Marcus region. On the other hand, clearly the rates of both ET and EPT decrease for lower temperatures.

The kinetic isotope effect of a PCET reaction will increase as the probability of the EPT mechanism increases and as the localization of and distance between the reactant and product proton vibrational wave functions increase. The reactant and product proton vibrational wave functions become more localized and separated as the proton donor−acceptor distance increases and as the electron donor−acceptor distance decreases (leading to stronger electron−proton Coulomb interactions). The probability of EPT becomes smaller while the distance between the reactant and product proton vibrational wave functions becomes larger as the proton donor−acceptor distance increases. As a result, the kinetic isotope effects are largest for intermediate proton donor−acceptor distances. In some cases, unusually large kinetic isotope effects may be observed for systems in which the EPT mechanism dominates. These large kinetic isotope effects are due to the electron−proton Coulomb interaction, which leads to proton vibrational wave functions that are highly localized near the proton donor or acceptor. Also, the probability of EPT is larger for hydrogen than for deuterium, further increasing the kinetic isotope effect.

Experimental studies on model PCET systems will play a critical role in the further development of this theoretical formulation of PCET. In particular, systematic experimental studies may be used to test our predictions concerning the impact of solute and solvent properties on the rates and kinetic isotope effects of PCET reactions. The analysis presented in this paper may aid in the design of more experimental model systems dominated by the EPT mechanism. In addition, the existing experimental data on PCET systems may be interpreted within the theoretical framework presented in this paper. Current research is directed at using the multistate continuum theory combined with electronic structure and electrostatic continuum methods to model specific systems that have been studied experimentally.

Acknowledgment. The authors thank Alexander Soudackov for many helpful discussions about this work. Financial support was provided by the NSF CAREER Program Grant CHE-9623813 and the Clare Boothe Luce Foundation. S.H.-S. is the recipient of an Alfred P. Sloan Foundation Research Fellowship and a Camille Dreyfus Teacher-Scholar Award.

References and Notes

(1) Babcock, G. T.; Barry, B. A.; Debus, R. J.; Hoganson, C. W.; Atamian, M.; McIntosh, L.; Sithole, I.; Yocum, C. F. *Biochemistry* **1989**, *28*, 9557. Okamura, M. Y.; Feher, G. *Annu. Rev. Biochem.* **1992**, *61*, 861. Kirmaier, C.; Holten, D. *The Photosynthetic Bacterial Reaction Center - - Structure and Dynamics*; Plenum: New York, 1988.

(2) Wikstrom, M. *Nature* **1989**, *338*, 776. Babcock, G. T.; Wikstrom, M. *Nature* **1992**, *356*, 301. Malmstrom, B. G. *Acc. Chem. Res.* **1993**, *26*, 332.

(3) Therien, M. J.; Selman, M.; Gray, H. B.; Chang, I.-J.; Winkler, J. R. *J. Am. Chem. Soc.* **1990**, *112*, 2420. Onuchic, J. N.; Beratan, D. N. *J. Chem. Phys.* **1990**, *92*, 722.

(4) Siegbahn, P. E. M.; Eriksson, L.; Himo, F.; Pavlov, M. *J. Phys. Chem. B* **1998**, *102*, 10622. Sjoberg, B. M.; Ekberg, M.; Persson, A.; Sahlin, M. *J. Inorg. Biochem.* **1999**, *74*, 51.

(5) Hirst, J.; Duff, J. L. C.; Jameson, G. N. L.; Kemper, M. A.; Burgess, B. K.; Armstrong, F. A. *J. Am. Chem. Soc.* **1998**, *120*, 7085.

(6) Marcus, R. A. *Annu. Rev. Phys. Chem.* **1964**, *15*, 155.

(7) Ulstrup, J. *Charge-Transfer Processes in Condensed Media*; Springer-Verlag: Berlin, 1979.

(8) Birge, R. R. *Annu. Rev. Phys. Chem.* **1990**, *41*, 683. Durr, H.; Bouas-Laurent, H. *Photochromism: Molecules and Systems. Studies in Organic Chemistry 40*; Elsevier: Amsterdam, 1990.

(9) Cukier, R. I.; Nocera, D. G. *Annu. Rev. Phys. Chem.* **1998**, *49*, 337.

(10) Turro, C.; Chang, C. K.; Leroi, G. E.; Cukier, R. I.; Nocera, D. G. *J. Am. Chem. Soc.* **1992**, *114*, 4013. Roberts, J. A.; Kirby, J. P.; Nocera, D. G. *J. Am. Chem. Soc.* **1995**, *117*, 8051.

(11) Kirby, J. P.; Roberts, J. A.; Nocera, D. G. *J. Am. Chem. Soc.* **1997**, *119*, 9230.

(12) Binstead, R. A.; Moyer, B. A.; Samuels, G. J.; Meyer, T. J. *J. Am. Chem. Soc.* **1981**, *103*, 2897. Binstead, R. A.; Meyer, T. J. *J. Am. Chem. Soc.* **1987**, *109*, 3287. Binstead, R. A.; McGuire, M. E.; Dovletoglou, A.; Seok, W. K.; Roecker, L. E.; Meyer, T. J. *J. Am. Chem. Soc.* **1992**, *114*, 173. Binstead, R. A.; Stultz, L. K.; Meyer, T. J. *Inorg. Chem.* **1995**, *34*, 546.

(13) Farrer, B. T.; Thorp, H. H. *Inorg. Chem.* **1999**, *38*, 2497.

(14) Roth, J. P.; Lovel, S.; Mayer, J. M. *J. Am. Chem. Soc.* **2000**, *122*, 5486.

(15) Soudackov, A. V.; Hammes-Schiffer, S. *J. Chem. Phys.* **1999**, *111*, 4672.

(16) Soudackov, A. V.; Hammes-Schiffer, S. *J. Am. Chem. Soc.* **1999**, *121*, 10598.

(17) Soudackov, A. V.; Hammes-Schiffer, S. *J. Chem. Phys.* **2000**, *113*, 2385.

(18) Hammes-Schiffer, S. Proton-Coupled Electron Transfer. In *Electron Transfer in Chemistry: Principles, Theories, Methods, and Techniques*; Balzani, V., Ed.; Wiley-VCH: Weinheim, Germany, 2001; Vol. I.

(19) Cukier, R. I. *J. Phys. Chem.* **1994**, *98*, 2377. Zhao, X. G.; Cukier, R. I. *J. Phys. Chem.* **1995**, *99*, 945. Cukier, R. I. *J. Phys. Chem.* **1995**, *99*, 16101; **1996**, *100*, 15428.

(20) Bianco, R.; Hynes, J. T. *J. Chem. Phys.* **1995**, *102*, 7864, 7885.

(21) Basilevsky, M. V.; Chudinov, G. E.; Newton, M. D. *Chem. Phys.* **1994**, *179*, 263−278.

(22) Warshel, A. *Computer Modeling of Chemical Reactions in Enzymes and Solutions*; John Wiley: New York, 1991.

(23) Kim, H. J.; Hynes, J. T. *J. Chem. Phys.* **1992**, *96*, 5088−5110.

(24) Zusman, L. D. *Chem. Phys.* **1980**, *49*, 295.

(25) Calef, D. F.; Wolynes, P. G. *J. Phys. Chem.* **1983**, *87*, 3387.

(26) Newton, M. D.; Friedman, H. L. *J. Chem. Phys.* **1988**, *88*, 4460. Liu, Y.-P.; Newton, M. D. *J. Phys. Chem.* **1995**, *99*, 12382.

(27) Hanggi, P.; Talkner, P.; Borkovec, M. *Rev. Mod. Phys.* **1990**, *62*, 251.

(28) Schmitt, U.; Voth, G. A. *J. Chem. Phys.* **1999**, *111*, 9361. The complete multistate EVB potential in this reference includes the interactions of the off-diagonal densities with the solvent. In the present paper, however, we use this EVB potential to describe only the two-state gas-phase protonated water dimer for which this interaction is not relevant. In other words, this EVB potential is used only as a tool to derive the functional form of the potential for our gas phase VB model for PCET. The interactions of the off-diagonal densities with the dielectric continuum solvent are neglected in the multistate continuum theory described in the present paper. This approximation allows us to obtain free energy surfaces as functions of only two scalar solvent coordinates for PCET reactions.

(29) Henderson, T. M.; Cave, R. J. *J. Chem. Phys.* **1998**, *109*, 7414.

(30) Westheimer, F. H.; Kirkwood, J. G. *J. Chem. Phys.* **1938**, *6*, 513.

(31) Marcus, Y. *Ion Solvation*; John Wiley: New York, 1985.

(32) Newton, M. D.; Sutin, N. *Annu. Rev. Phys. Chem.* **1984**, *35*, 437.

(33) Barbara, P. F.; Meyer, T. J.; Ratner, M. A. *J. Phys. Chem.* **1996**, *100*, 13148.